iScience

CellPress
OPEN ACCESS

Article

The serendipitous effect of KF in Ritter reaction: Photo-induced amino-alkylation of alkenes

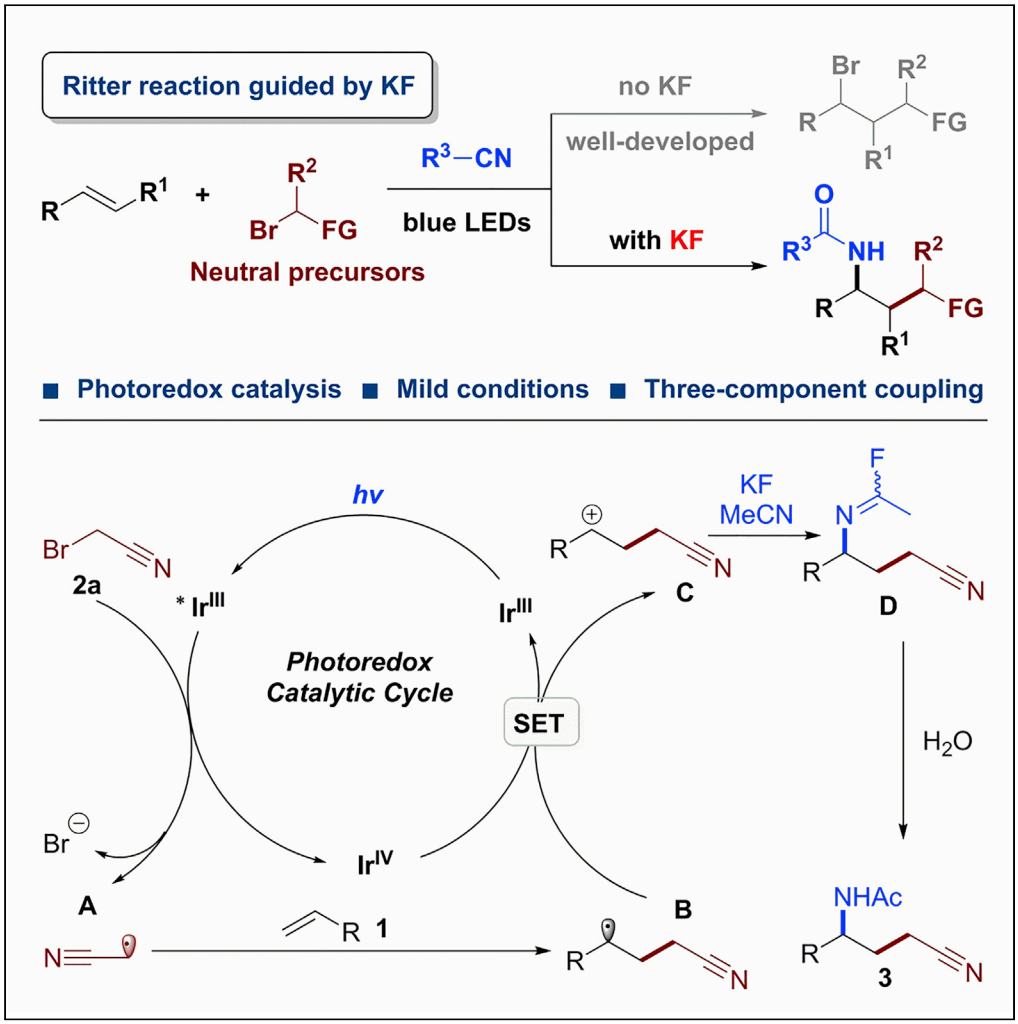

Yu-Qing Guan, Xiang-Ting Min, Gu-Cheng He, Ding-Wei Ji, Shi-Yu Guo, Yan-Cheng Hu, Qing-An Chen

qachen@dicp.ac.cn

Highlights

Using light irradiation to promote amino-alkylation of alkenes

Using KF to facilitate three-component Ritter reaction

Access functionalized amides under mild conditions

Guan et al., iScience 24, 102969
September 24, 2021
https://doi.org/10.1016/j.isci.2021.102969

iScience

CellPress
OPEN ACCESS

Article

The serendipitous effect of KF in Ritter reaction: Photo-induced amino-alkylation of alkenes

Yu-Qing Guan,[1] Xiang-Ting Min,[1,2] Gu-Cheng He,[1,2] Ding-Wei Ji,[1] Shi-Yu Guo,[1] Yan-Cheng Hu,[1] and Qing-An Chen[1,2,3,*]

SUMMARY

Ritter reaction has been recognized as an elegant strategy to construct the C−N bond. Its key feature is forming the carbocation for nucleophilic attack by nitriles. Herein, we report a complementary visible-light-induced three-component Ritter reaction of alkenes, nitriles, and α-bromo nitriles/esters, thereby providing mild and rapid access to various γ-amino nitriles/acids. Mechanistic studies indicated that traceless fluoride relay, transforming KF into imidoyl fluoride intermediate, is critical for the efficient reaction switch from atom transfer radical addition (ATRA) to the Ritter reaction. This approach to amino-alkylation of alkenes is chemoselective and operationally simple.

INTRODUCTION

Since its discovery in 1948 (Ritter and Kalish, 1948; Ritter and Minieri, 1948), Ritter reaction has been recognized as one of the most powerful methods for amide synthesis through the formation of the C−N bond (Scheme 1A) (Bolsakova and Jirgensons, 2017; Crouch, 1994; Guérinot et al., 2012; Jiang et al., 2014; Kürti and Czakó, 2005; Li-Zhulanov et al., 2020; Mohammadi Ziarani et al., 2020; Pronin et al., 2013; Qu et al., 2012; Zheng et al., 2015). This two-component protocol usually involves the generation of carbocation intermediates from tertiary, secondary, and benzylic alcohols under acidic conditions (Kürti and Czakó, 2005). As basic feedstock chemicals, simple alkenes have also been widely used as carbocation precursors in Ritter reaction (Eren and Kusefoglu, 2005; Huang et al., 2012; Jiang and Studer, 2020; Nandy et al., 2020; Park et al., 2018; Shi et al., 2015; Subba Reddy et al., 2010; Welniak, 1996; Williams et al., 2017; Xu et al., 2017; Yang et al., 2018; Yasuda and Obora, 2015; Zhang et al., 2020). Of particular interest is the three-component Ritter reaction, which can efficiently incorporate two distinct functional groups onto the carbon-carbon double bonds in one-step (Abe et al., 2010, 2017; Ahmed et al., 2020; Ai et al., 2015; Bao et al., 2019; Chen et al., 2016; Feng et al., 2018; Liu and Klussmann, 2020; Qian et al., 2017; Zhu et al., 2017). Nowadays, photoredox catalysis (Hopkinson et al., 2016; Marzo et al., 2018; Narayanam and Stephenson, 2011; Prier et al., 2013; Romero and Nicewicz, 2016; Shaw et al., 2016; Skubi et al., 2016; Tellis et al., 2016; Twilton et al., 2017; Xuan and Xiao, 2012; Yu et al., 2020, 2021) for simultaneously constructing C−C and C−X bonds has become a new paradigm of alkene difunctionalizations (Badir and Molander, 2020; Chen et al., 2018; Koike and Akita, 2016; Lipp et al., 2021; Protti et al., 2016; Yin et al., 2020; Zhu et al., 2020). With the help of cationic precursors (Umemoto's reagent, iodonium salt, or diazonium salt), Akita, Greaney, and König developed elegant three-component Ritter reactions of alkenes under visible light irradiation (Scheme 1B) (Fumagalli et al., 2013; Prasad Hari et al., 2014; Yasu et al., 2013; Zong et al., 2019). Notably, the introduction of a corresponding counterion (BF_4^-) with weak nucleophilicity could spare the active carbocation intermediates to be exclusively attacked by nitrile partners. Therefore, the development of photo-induced Ritter reaction from neutral precursors with competitive nucleophiles is challenging and appealing.

As is well known, photo-induced atom transfer radical addition (ATRA) with neutral precursors is a well-established protocol for alkene difunctionalizations (Courant and Masson, 2016; Magagnano et al., 2017; Mao and Cong, 2017; Ouyang et al., 2018; Pu et al., 2019; Rawner et al., 2018). The high chemoselectivity of ATRA is mostly attributed to the existence of a single nucleophile which attacked carbocation. Regarding the use of the widely available alkylbromides as precursors for carbocation intermediates in the Ritter reaction, which nucleophile would display stronger affinity toward carbocation, bromides or nitriles? Intrigued by the aforementioned issue and our long-standing interests in functionalization of alkenes (Ji et al., 2019; Jiang et al., 2021; Kuai et al., 2020; Min et al., 2021; Yang et al., 2019), we sought to develop photo-induced three-component Ritter reaction of alkenes with alkylbromides and nitriles.

[1]Dalian Institute of Chemical Physics, Chinese Academy of Sciences, Dalian 116023, China

[2]University of Chinese Academy of Sciences, Beijing 100049, China

[3]Lead contact

*Correspondence: qachen@dicp.ac.cn

https://doi.org/10.1016/j.isci.2021.102969

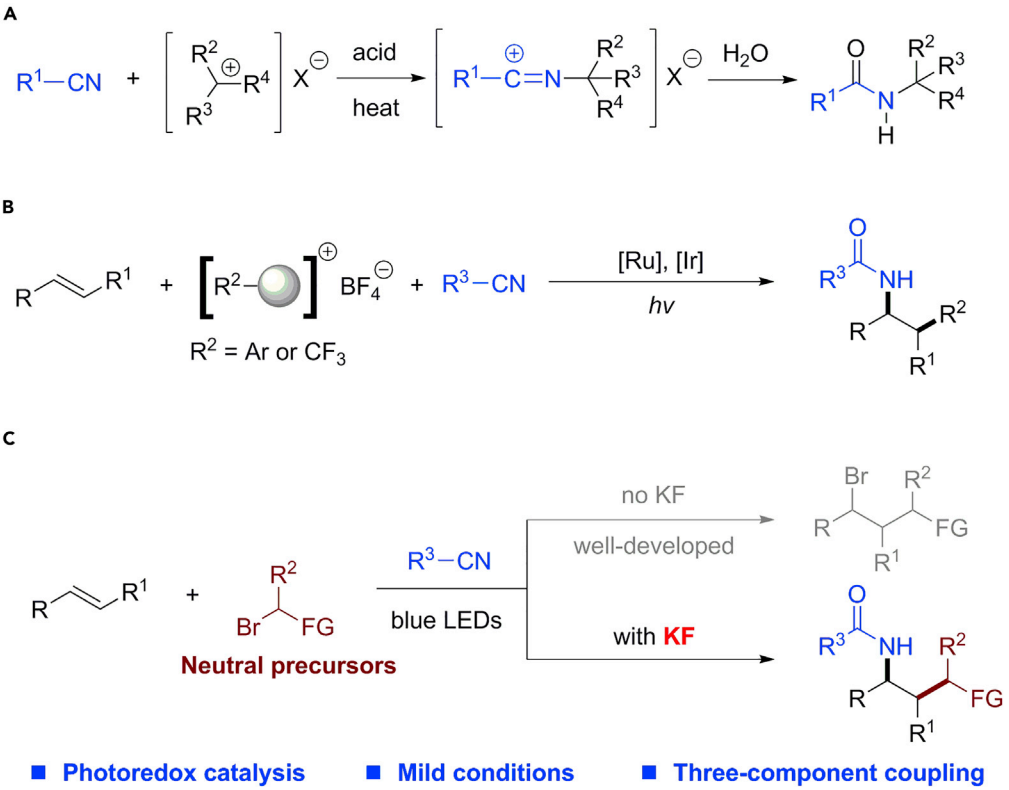

Scheme 1. Design of photo-induced three-component Ritter reaction via fluoride

(A) Classic Ritter reaction for the synthesis of amides.

(B) Previous work: photo-induced Ritter reaction with cationic precursors.

(C) This work: inorganic fluoride-induced chemoselective Ritter reaction.

Herein, we demonstrated an unprecedented role of fluoride salts for the enhancement of Ritter reaction and inhibition of ATRA (Scheme 1C).

RESULTS

Optimization reaction conditions

Initially, with $Ir(ppy)_3$ (1 mol%) as a photocatalyst, styrene (**1a**) and 2-bromoacetonitrile (**2a**) were chosen as the model substrates to test our hypothesis (see Tables 1, S1). Without any additive, ATRA of **1a** proceeded smoothly as expected to give 4-bromo-4-phenylbutanenitrile (**4a**) at 71% yield (entry 1). Despite the favor for **4a**, the use of KBF_4 as the additive accidentally gave **3a** as a minor product (entry 2). It inspired us to use other additives containing fluorine atoms (entries 3–8). Trifluoroacetic acid (TFA) showed no enhancement on the selectivity of **3a** (entry 3). Fortunately, $NEt_3{\cdot}3HF$ and NaF could facilitate the formation of γ-amino nitrile (**3a**) with moderate selectivity (entries 4 and 5). Particularly, KF and CsF proved to be suitable additives and the target product **3a** was delivered in satisfactory yields and good selectivity (entries 6–7). In the case of quaternary ammonium salt NBu_4F, the reaction did not occur (entry 8). With respect to the anion effect of additives, potassium salts with other halide ions (KCl, KBr, and KI) contrarily gave **4a** as the main product (entries 9–11). The aforementioned results showed the significance of fluoride anion for high selectivity of **3a**. Other common metallaphotoredox catalysts, such as $[Ir(ppy)_2dtbbpy]PF_6$ and $[Ru(bpy)_3]Cl_2$, yielded no desired product **3a** (entries 12 and 13). When switching to organic photocatalyst Eosin Y, the reaction could not take place (entry 14). In addition, the control experiments confirmed the essential roles of the iridium catalyst and the visible light irradiation for this protocol (entries 15 and 16). If H_2O was present from the beginning in the similar condition under air atmosphere, **3a** was obtained in 57% yield, albeit with a small amount of 4-hydroxy-4-phenylbutyronitrile (entry 17). No **3a** was observed in the absence of KF (entry 18). The aforementioned results indicate that KF plays an indispensable role to create target product **3a**.

Table 1. Selected optimization studies

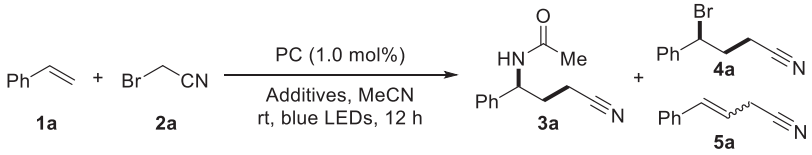

			Yield (%)[a]		
Entry	Photocatalyst	Additive	3a	4a	5a
1	$Ir(ppy)_3$	–	1	71	6
2	$Ir(ppy)_3$	KBF_4	8	59	7
3[b]	$Ir(ppy)_3$	TFA	5	73	1
4[c]	$Ir(ppy)_3$	$NEt_3 \cdot 3HF$	51	22	6
5	$Ir(ppy)_3$	NaF	63	12	9
6	**$Ir(ppy)_3$**	**KF**	**95**	**0**	**0**
7	$Ir(ppy)_3$	CsF	85	0	1
8	$Ir(ppy)_3$	NBu_4F	–	–	–
9	$Ir(ppy)_3$	KCl	16	37	13
10	$Ir(ppy)_3$	KBr	0	63	19
11	$Ir(ppy)_3$	KI	1	12	5
12	$[Ir(ppy)_2(dtbbpy)]PF_6$	KF	0	7	1
13	$[Ru(bpy)_3]Cl_2$	KF	0	8	0
14	Eosin Y	KF	–	–	–
15	–	KF	–	–	–
16	$Ir(ppy)_3$ (In dark)	KF	–	–	–
17[d]	$Ir(ppy)_3$ (air, H_2O)	KF	57	0	1
18[d]	$Ir(ppy)_3$ (air, H_2O)	–	0	55	2

[a]Reaction conditions: **1a** (0.21 mmol), **2a** (0.20 mmol), photocatalyst (1.0 mol%), additives (0.40 mmol), MeCN (0.8 mL), rt, under N_2, 10 W blue LEDs, 12 h. Yields were determined by ^1H NMR spectroscopy using 1,3,5-trimethoxybenzene as the internal standard. See also Tables S1.
[b]TFA = trifluoroacetic acid, 0.3 equiv.
[c]1.0 equiv.
[d]H_2O (3.0 equiv.) was added.

Substrate scope study

With the optimized conditions in hand, the generality of alkene substrates was subsequently investigated. As shown in Figure 1, various substituted styrenes were suitable for this photo-induced Ritter reaction, affording γ-cyano acetamides with moderate to excellent yields. Aryl alkenes **1** bearing substituents at *para* position, such as Me, ^{t}Bu, and Ph groups, all afforded the desired products in good yields (83–99%, **3b**-**3d**, **3i**). Substrates with halides, including F, Cl, or Br on the phenyl ring, were well tolerated under the current protocol regardless of the substitution position (**3e**-**3g**, **3j**-**3l**). It should be noted that benzyl chloride, which was easily attacked by nucleophiles, also remained intact, giving the target product an 84% yield (**3h**). When a naphthyl alkene was subjected to the standard condition, the corresponding product **3m** was obtained in moderate yield. Notably, 1,2-disubstituted alkenes such as cyclic (**3n**) and acyclic alkenes (**3o**) were well compatible to give desired products in good yields with acceptable diastereoisomeric ratios (dr).

In order to enrich the category of products, we next studied substrate scope with respect to radical precursors, α-bromoesters (Figure 2). Substituted vinylarenes with the Br or Cl group all reacted successfully with ethyl bromoacetate, furnishing the target products with moderate to good yields (**6a**-**6e**). The molecular structure of **6b** was confirmed by X-ray crystallographic analysis. Interestingly, α-substituted C-radicals bearing

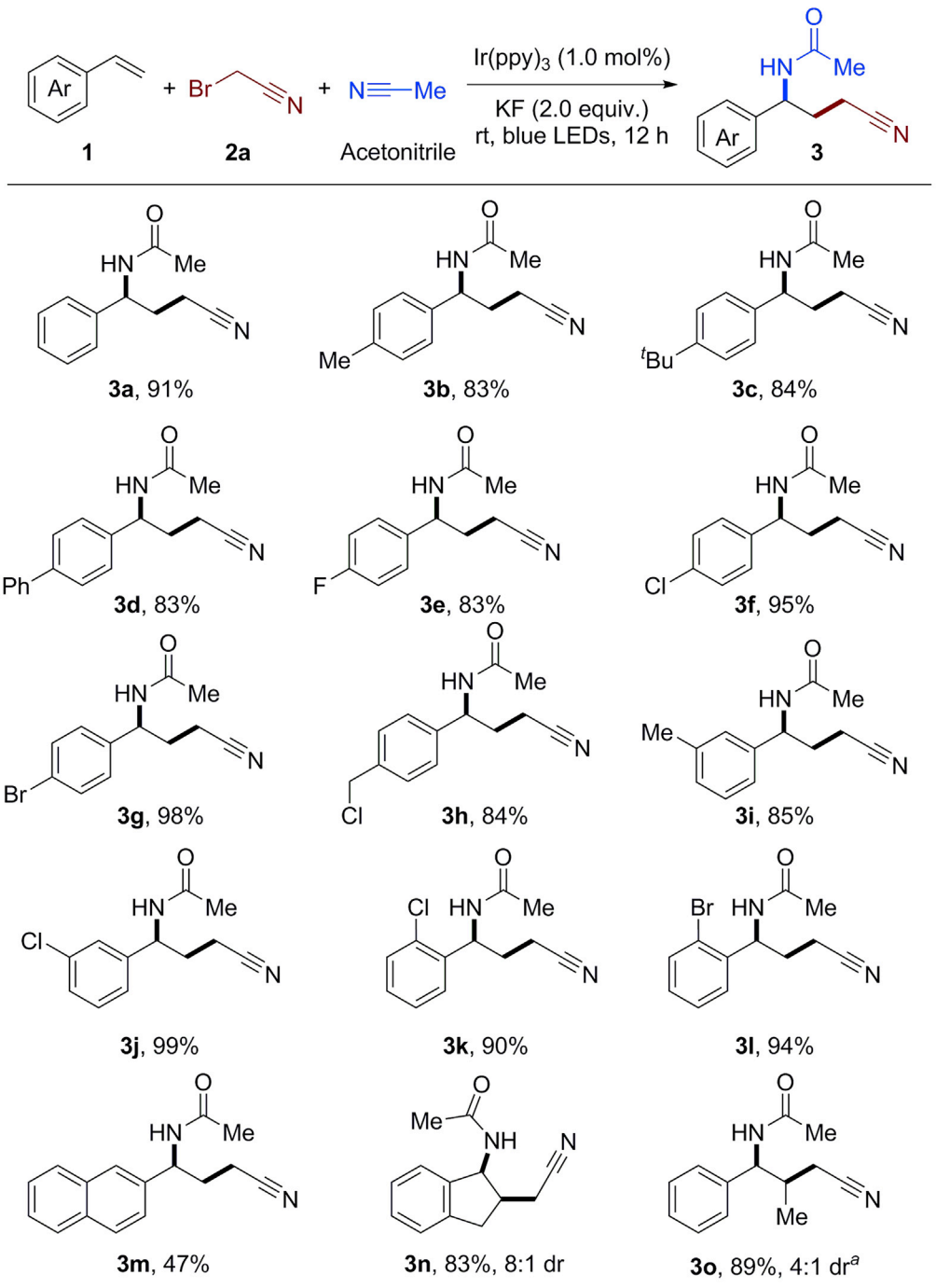

Figure 1. Substrate scope with respect to alkenes

Reaction conditions: **1** (0.21 mmol), **2a** (0.20 mmol), $Ir(ppy)_3$ (1.0 mol%), KF (0.40 mmol), MeCN (0.8 mL), rt, under N_2, 10 W blue LEDs, 12 h. Isolated yield was given. Diastereoisomeric ratio (dr) was determined by ^1H NMR analysis.

electron-withdrawing groups such as mono-fluoro, *gem*-difluoro groups worked well to provide the corresponding products **6f**-**6i** in 37–68% yields. In the case of methyl 2-bromopropanoate, the product **6j** was isolated at 45% yield, together with 3:1 dr. Furthermore, the reaction with phenyl 2-bromoacetate also performed smoothly to give the desired product with 63% yield (**6k**).

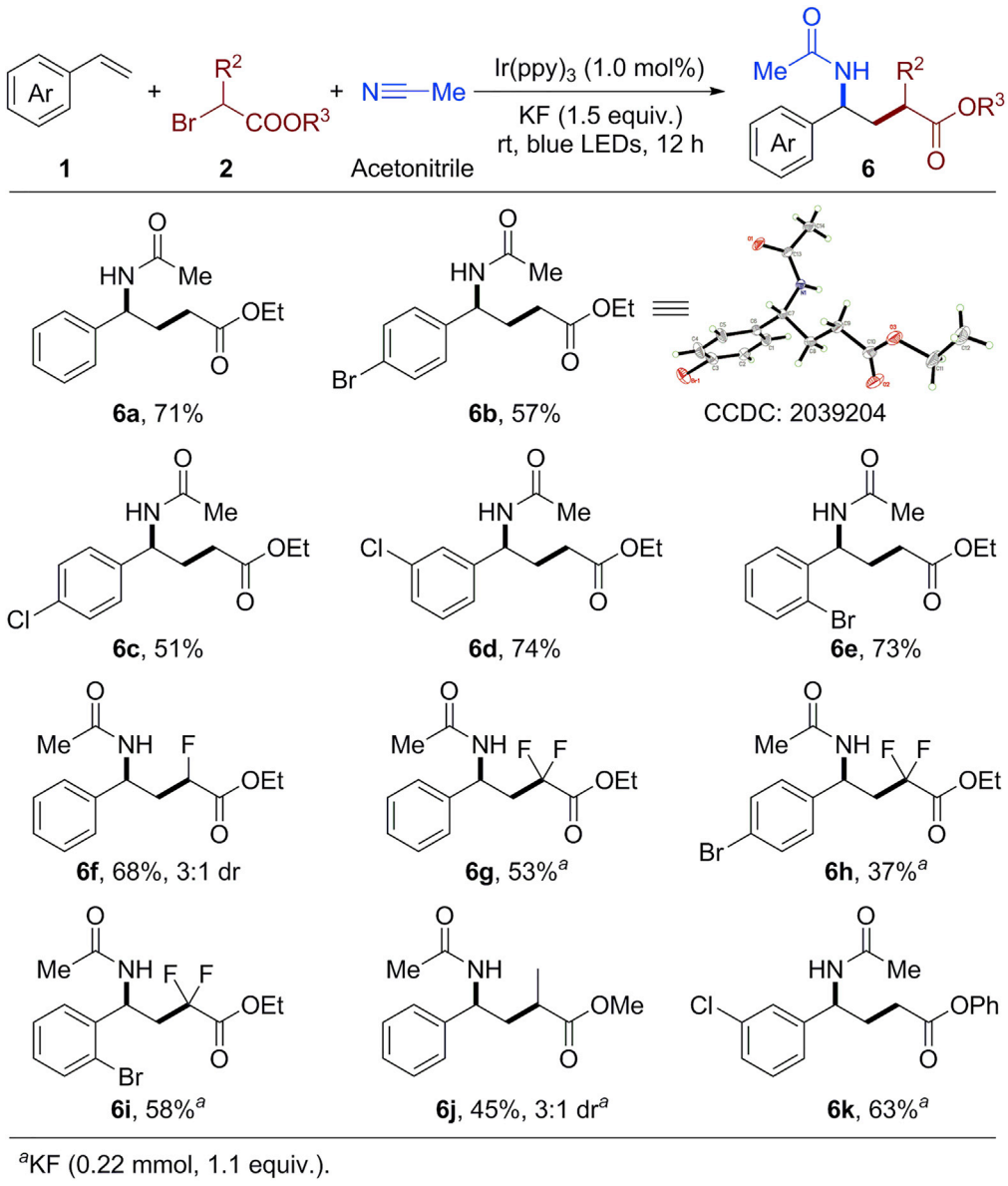

Figure 2. Substrate scope with respect to radical precursors

Reaction conditions: **1** (0.21 mmol), **2a** (0.20 mmol), $Ir(ppy)_3$ (1.0 mol%), KF (0.30 mmol), MeCN (0.8 mL), rt, under N_2, 10 W blue LEDs, 12 h. Isolated yield was given. Diastereoisomeric ratio (dr) was determined by ^1H NMR analysis.

In addition, various nitriles were evaluated as well (Figure 3). To our delight, benzonitrile was a suitable partner, giving rise to the product **8a** with a 46% yield. In terms of reactions with *o*- and *m*-tolunitriles, CsF was found to be a better additive (**8b**, **8c**). Under the similar conditions, isobutyronitrile and valeronitrile could also be readily transformed into the corresponding products (**8d**, **8e**) in moderate yields. Isovaleronitrile was also applicable to the process, forming the product **8f** with 46% yield. Especially, bulkier pivalonitrile also worked to afford the product **8g** with 32% yield. These lower yields than that of acetonitrile might be attributed to steric hindrance and weaker nucleophilic ability.

Scale-up synthesis and transformations

To demonstrate the potential utility of this methodology, a gram scale reaction of **1a** and **2a** in acetonitrile was performed. We were glad to find that product **3a** was obtained with high yield even when the catalyst loading of $Ir(ppy)_3$ was decreased to 0.2 mol% (Scheme 2A). In addition, further synthetic transformations of

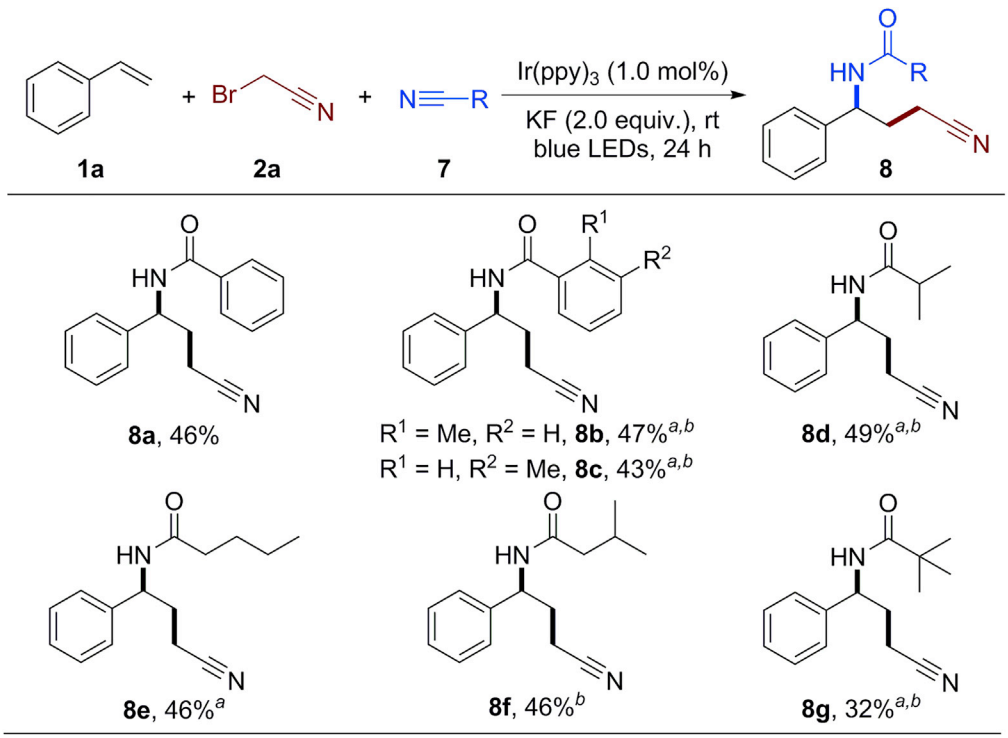

Figure 3. Substrate scope with respect to nitriles

Reaction conditions: **1a** (0.21 mmol), **2a** (0.20 mmol), $Ir(ppy)_3$ (1.0 mol%), KF (0.40 mmol), nitriles **7** (0.8 mL), rt, under N_2, 10 W blue LEDs, 12 h. Isolated yield was given.

the products toward cyclic amine and amide were studied (Scheme 2B). By using commercially available acetaldoxime and nickel salts in water, **3a** was hydrated into the corresponding amide **9** with 64% yield (Ma et al., 2012). A treatment of **3a** with sodium in butanol delivered 2-phenylpyrrolidine **10** with 76% yield (Zhu et al., 2017). In the presence of Cs_2CO_3, γ-amino ester **6a** could be readily transformed into 5-phenylpyrrolidin-2-one **11** with 81% yield.

DISCUSSION

Mechanism of the study

To probe the importance of photonic input, the light dependence of the reaction was examined (see Table S3 and Figure S81 for light on/off experiments). It is shown that continuous irradiation of visible light is required for effective formation of product **3a** which rapidly ceases in the absence of light. Furthermore, we calculated a quantum yield value (Cismesia and Yoon, 2015) of $\Phi = 0.35$ (see Figures S82 and S83). This observation indicates that this protocol probably does not involve a light-initiated radical chain pathway.

Next, several control experiments have been conducted to probe into the generation of carbocation intermediates under this protocol. When CD_3CN was used as the solvent, the target deuterated product **3a-d_3** was obtained in 97% yield with >99% deuterium at the methyl group (Scheme 3A). This deuterium labeling result indicates that 2-bromo-acetonitrile **2a** serves as a radical precursor and the carbocation intermediate is exclusively trapped by acetonitrile. Instead of **3a**, 4-methoxy-4-phenylbutane-nitrile **12** was formed at 90% yield in the presence of methanol. The stronger nucleophilicity of methanol brought about this product variation supporting the existence of conceivable carbocation intermediate (Scheme 3B). In the presence of radical scavenger [(2,2,6,6-tetramethylpipe-ridin-1-yl)oxyl] (TEMPO), the reaction was totally suppressed. This radical trapping experiment suggests that a radical pathway is probably involved for generation of carbocation intermediates (Scheme 3C).

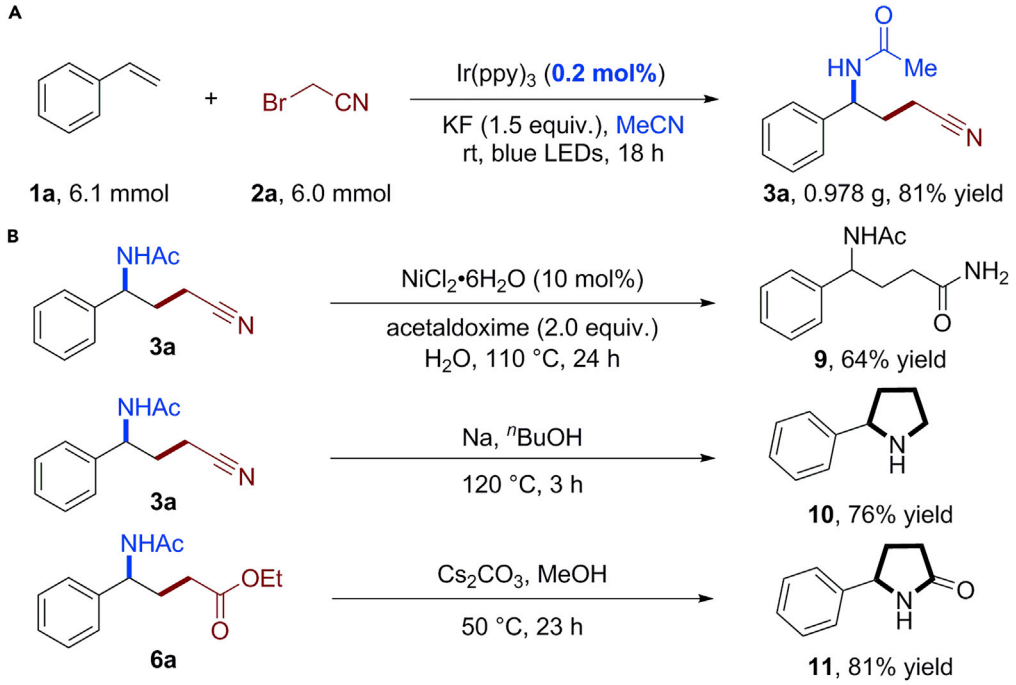

Scheme 2. Gram-scale reaction and synthetic transformations

(A) Gram-scale reaction with low catalyst loading.

(B) Synthetic transformations.

Encouraged by these significant results on the nature of the photo-induced Ritter reaction, we were curious about the effect of KF. The usage amount of KF on the control of product selectivity was further examined (Figure 4A, Table S2). ATRA product **4a** was favored as a major product in the absence of KF. With the

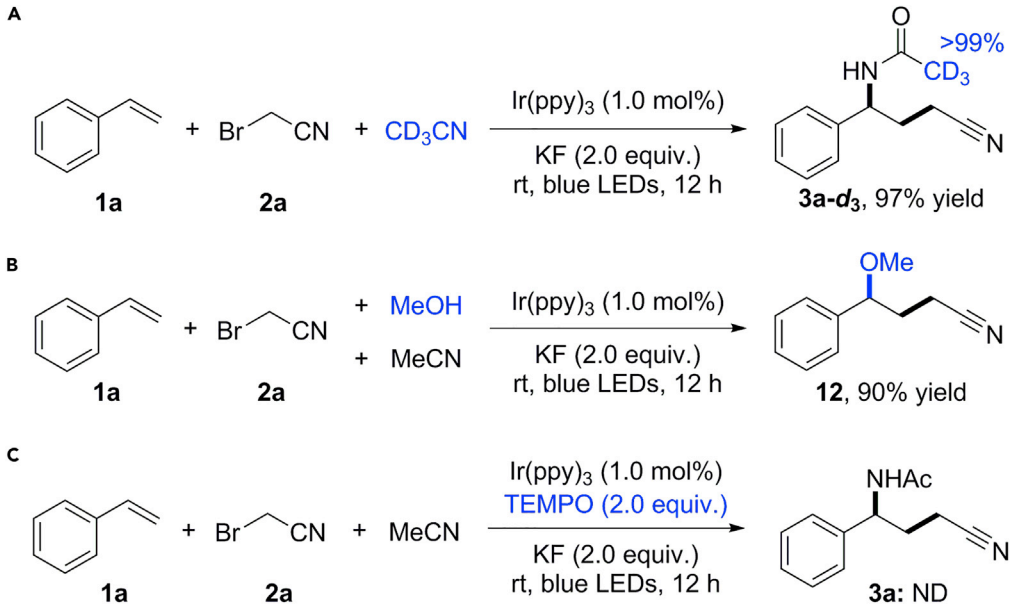

Scheme 3. Mechanistic studies regarding the carbocation intermediate

(A) Deuterium labeling experiment.

(B) Carbocation attacked by heteroatom nucleophiles.

(C) Radical trapping experiment. See also Schemes S1–S3.

A The usage amount of KF on the control of product selectivity

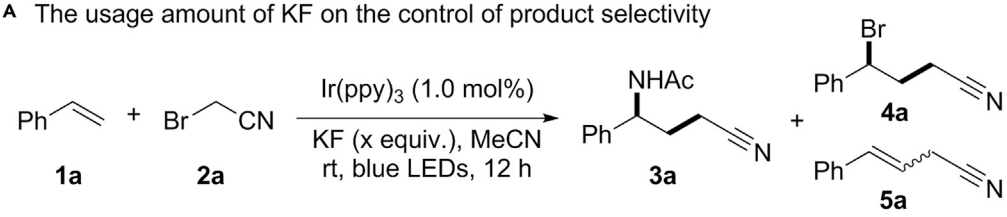

entry	KF (x equiv.)	yield (%) 3a	4a	5a
1	0	trace	71	6
2	0.5	23	46	22
3	1.0	59	16	trace
4	1.5	91	0	trace
5	2.0	95	0	0

B Key elements on the photo-induced substitution of **4a** to **3a**

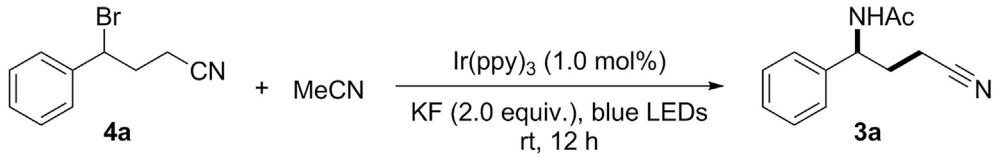

entry	Variation from the above conditions	yield (%)
1	none	77
2	no [Ir]	NR
3	no light	NR
4	no KF	NR

C Control experiment of **12**

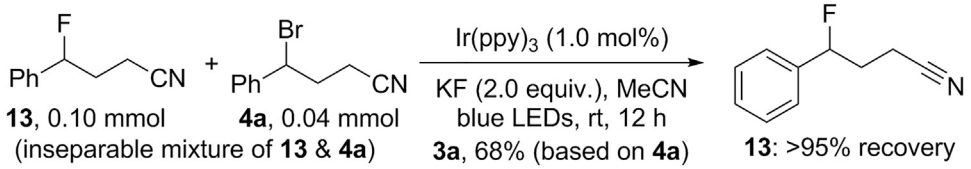

Figure 4. The effect of fluoride on the product selectivity

increasing loading of KF (0.5–2.0 equiv.), product **3a** gradually dominated in the product distributions (23–95% yield). Taken together, we wondered whether **4a** could be transformed into **3a** with appropriate use of KF. Thus, the transformation of **4a** was carried out under the standard condition (Figure 4B, entry 1, Table S4). As expected, product **3a** was isolated at 77% yield after 12 h. In the absence of the iridium catalyst, visible light irradiation, or KF, no **3a** was generated (entries 2–4). These results suggest that KF plays an important role in the orientation of intermediate trapping to control product selectivity. Furthermore, the inseparable mixture of 4-fluoro-4-phenylbutyronitrile **13** and **4a** as reactants were carried out with the standard condition. As a result, **13** showed an inert substrate and was fully recovered (Figure 4C and Scheme S5). This observation suggests **13** is not the resting intermediate for the formation of target product **3a**.

Given the dramatic effect of KF on the product selectivity (Figure 4), the fate of fluoride during the reaction was further investigated (Figure 5). Fortunately, fluorine-19 nuclear magnetic resonance (^{19}F NMR) provides an effective means for analyzing fluoride species. The comparison of ^{19}F NMR spectra between 0 and

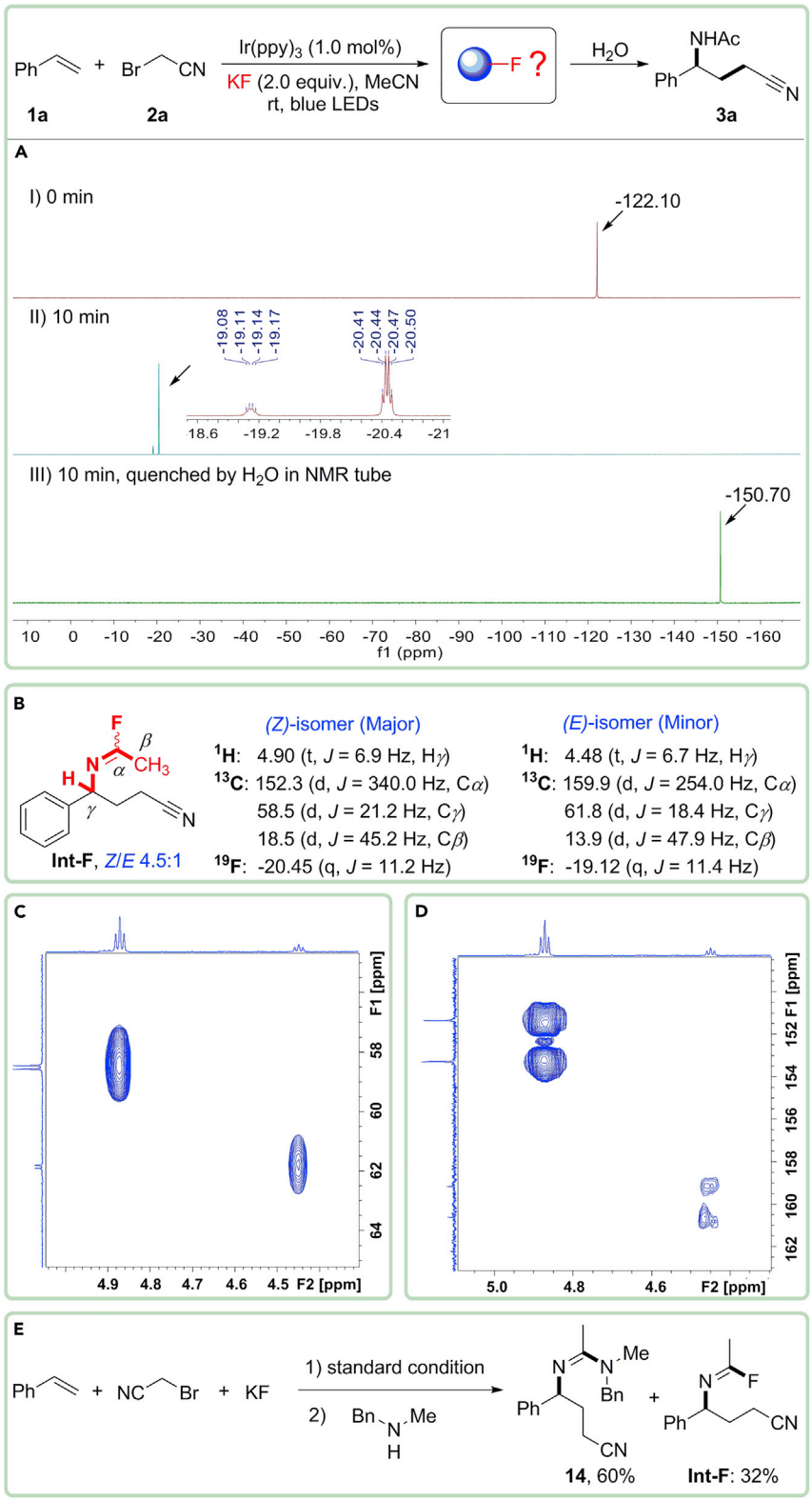

Figure 5. The characterization of the fluoride intermediate

(A) ^{19}F NMR spectra of reaction mixture at different reaction stages.

(B) Summarized chemical shifts and spin coupling constants for the fluoride intermediate.

Figure 5. *Continued*
(C) HMQC spectrum at 10 min.
(D) HMBC spectrum at 10 min.
(E) Further transformation of imidoyl fluoride.

10 min showed a clear change from −122.10 ppm to −20.45 ppm (Figures 5A, I, II, S93, and S96). This downfield shift suggests a strong decrease of electron density on fluorine atoms. Both F signals (−19.12 and −20.45 ppm) were split into a quartet with similar coupling constants (11.2 and 11.4 Hz), indicating the existence of three neighboring hydrogen atoms (Figure 5B). These characteristics suggest the mysterious intermediate is an organic fluoride.

Subsequently, ^{1}H, ^{13}C, ^{19}F NMR, ^{1}H-^{13}C heteronuclear multiple quantum coherence (HMQC), and ^{1}H-^{13}C heteronuclear multiple bond correlation (HMBC) spectra were collected for comprehensive analysis of the structure of fluoride intermediate (see Figures S94–S98). To cut a long story short, representative chemical shifts and coupling constants are summarized in Figure 5B. Notably, ^{13}C NMR spectra displayed two sets of doublets at 152.3 and 159.9 ppm characterized by very large $^{1}J_{C\text{-}F}$ coupling constants (340.0 and 254.0 Hz). Obvious remote heteronuclear *J*-couplings ($^{2}J_{C\text{-}F}$ and $^{3}J_{C\text{-}F}$) were also observed at the aliphatic carbon region (13.9, 18.5, 58.5, and 61.8 ppm). The analysis of ^{1}H-^{13}C HMQC and ^{1}H-^{13}C HMBC spectra (Figures 5C and 5D) was carried out to determine the space connectivity between diagnostic carbons (58.5, 61.8 152.3, and 159.9 ppm) and hydrogens (4.90 and 4.48 ppm). With these self-consistent correlations, we inferred a formation of imidoyl fluoride intermediate **Int-F**. The significant difference in the $^{1}J_{C\text{-}F}$ coupling constants (340.0 and 254.0 Hz) probably results from the geometrical effect (*Z*/*E* isomers) of **Int-F** on the heteronuclear Cα−F interaction (Norell, 1970; Rowe et al., 1999). Moreover, ^{1}H NMR, ^{13}C NMR, ^{1}H-^{13}C HMQC, and ^{1}H-^{13}C HMBC spectra were collected and analyzed to further support the proposed imidoyl fluoride **Int-F** using CD_3CN as the deuterium-labeling reactant (see Figures S99–S103). Eventually, the desired product **3a** was generated from the quench of intermediate **Int-F** by H_2O in the NMR tube (see Figures S104–S106). Meanwhile, a dramatic upfield shift in ^{19}F NMR from −20.45 ppm to −150.70 ppm also suggests the cleavage of the Cα−F bond on intermediate **Int-F** (Figures 5A, III, and S106). In addition, intermediate **Int-F** could be captured by *N*-methylbenzylamine to afford the corresponding amidine **14** (Gurjar and Fokin, 2020) in 60% NMR yield (Figures 5E, S107, and S108). This result further supports the formation of intermediate **Int-F**.

Based on the aforementioned results and literature reports on photo-induced reactions (Courant and Masson, 2016; Fumagalli et al., 2013; Prasad Hari et al., 2014; Yasu et al., 2013; Zong et al., 2019), a plausible mechanism is shown in Scheme 4. Metallaphotoredox catalyst $Ir(ppy)_3$ ($E_{1/2}^{M+/M*}$ = −1.73 V vs. SCE) (Shih et al., 2010) is excited by visible light irradiation to generate the excited species $*Ir^{III}$. A subsequent single-electron transfer (SET) process (Yi et al., 2014) yields acetonitrile radical **A** (bromoacetonitrile: $E_{1/2}^{red}$ = −0.69 V vs. SCE) (Isse and Gennaro, 2004), a bromide anion and Ir^{IV} species. Then the radical addition of **A** onto alkene **1** affords the C−C coupling adduct **B**, which is oxidized by the Ir^{IV} to form the carbocation intermediate **C** through another SET process. Intermediate acetimidoyl fluoride **D** is generated from the nucleophilic attack of acetonitrile onto carbocation **C**. The final hydrolysis workup delivers the expected product **3**. Alternatively, atom transfer radical addition between bromo nitrile **2a** and alkene **1** yields the adduct **4** which can return the cycle through a photoredox pathway. Side product **5** could be generated from the β-proton elimination of carbocation **C**.

Conclusion

In conclusion, we have developed a three-component Ritter reaction of alkenes, nitriles, and alkylbromides through photoredox catalysis. A variety of synthetically useful γ-amino nitriles/acids were easily prepared. Through the selective capture of carbocation by nitrile and KF, the formation of imidoyl fluoride intermediate diverts the reaction from undesired atom transfer radical addition to the expected Ritter reaction. The salient features of this protocol include mild reaction conditions, good synthetic utility, and easy scalability. This photoredox catalysis serves as a complementary protocol for conventional thermal or acid-promoted Ritter reaction. Further investigations on the utilization of this mild approach are in progress in our laboratory.

Limitations of the study

The 1,1-disubstituted styrenes, alkyl-substituted alkenes, and other alkyl halides were not suitable in this methodology (See Figure S85 for details).

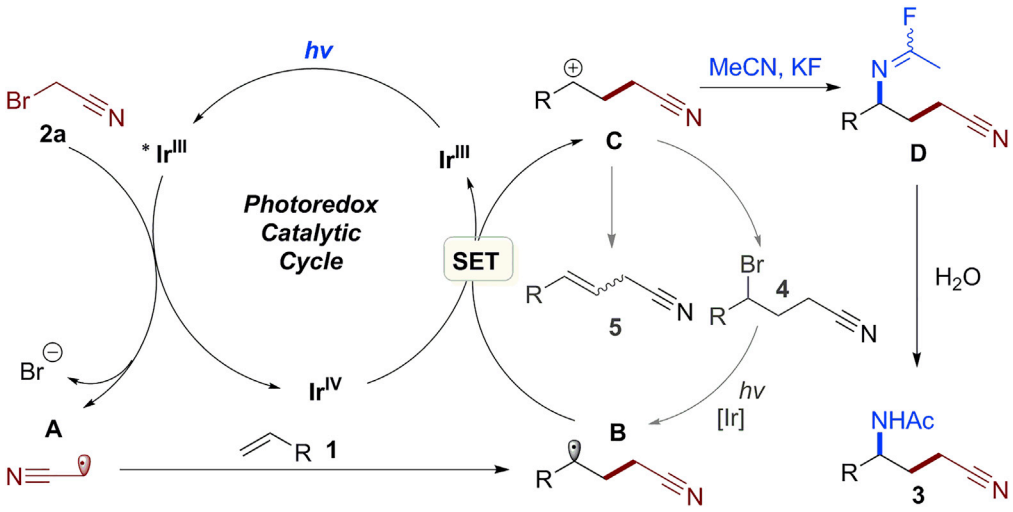

Scheme 4. Proposed mechanism

STAR★METHODS

Detailed methods are provided in the online version of this paper and include the following:

- KEY RESOURCES TABLE
- RESOURCE AVAILABILITY
  - Lead contact
  - Materials availability
  - Data and code availability
- METHOD DETAILS
  - Initial trials and reaction optimization (see Table S1)
  - General procedure A
  - Light on/off experiments
  - Quantum yield measurements
  - Characterization of products **3a**-**3o**
  - Characterization of products **6a**–**6k**
  - Characterization of products **8a**–**8g**
  - Gram-scale reaction
  - Synthetic transformations
  - Mechanistic study
  - Control experiments

SUPPLEMENTAL INFORMATION

Supplemental information can be found online at https://doi.org/10.1016/j.isci.2021.102969.

ACKNOWLEDGMENTS

We are grateful for the Dalian Institute of Chemical Physics (DICPI201902), Dalian Outstanding Young Scientific Talent, and China Postdoctoral Science Foundation (2019M661137) for financial support. We thank Xiujuan Chi (DICP) for expert advice with the NMR spectroscopic measurements.

AUTHOR CONTRIBUTIONS

Q.-A.C conceived and supervised the project. Y.-Q.G. discovered the reported process and designed and carried out almost all the experiments. X.-T.M. participated in synthesizing partial Ritter products and synthetic transformations. G.-C.H. synthesized partial Ritter products. D.-W.J. and S.-Y.G. helped in analyzing

the data. Y.-Q.G., Y.-C.H., and Q.-A.C wrote the manuscript. Y.-Q.G. wrote supporting information. All the authors discussed the results and commented on the manuscript.

DECLARATION OF INTERESTS

The authors declare no competing interests.

Received: May 27, 2021
Revised: July 28, 2021
Accepted: August 6, 2021
Published: September 24, 2021

REFERENCES

Abe, T., Kida, K., and Yamada, K. (2017). A copper-catalyzed ritter-type cascade via iminoketene for the synthesis of quinazolin-4(3H)-ones and diazocines. Chem. Commun. *53*, 4362–4365.

Abe, T., Takeda, H., Miwa, Y., Yamada, K., Yanada, R., and Ishikura, M. (2010). Copper-catalyzed Ritter-type reaction of unactivated alkenes with dichloramine-T. Helv. Chim. Acta *93*, 233–241.

Ahmed, W., Zhang, S., Feng, X., Yu, X., Yamamoto, Y., and Bao, M. (2020). Cooperative catalysis of copper, silver, and Brønsted acid for three-component carboamination of arylalkenes with allylic alcohols and nitriles. ChemCatChem *12*, 5200–5208.

Ai, W., Shi, R., Zhu, L., Jiang, D., Ma, X., Yuan, J., and Wang, Z. (2015). One-pot protocol to synthesize *N*-(*β*-nitro)amides by tandem Henry/Ritter reaction. RSC Adv. *5*, 24044–24048.

Badir, S.O., and Molander, G.A. (2020). Developments in photoredox/nickel dual-catalyzed 1,2-difunctionalizations. Chem *6*, 1327–1339.

Bao, H., Zhou, B., Jin, H., and Liu, Y. (2019). Copper-catalyzed three-component reaction of *N*-heteroaryl aldehydes, nitriles, and water. Org. Biomol. Chem. *17*, 5021–5028.

Bolsakova, J., and Jirgensons, A. (2017). The Ritter reaction for the synthesis of heterocycles. Chem. Heterocycl. Compd. *53*, 1167–1177.

Chen, G.-G., Wei, J.-Q., Yang, X., and Yao, Z.-J. (2016). Convenient one-step synthesis of benzo[c]phenanthridines by three-component reactions of isochromenylium tetrafluoroborates and stilbenes in acetonitrile. Org. Lett. *18*, 1502–1505.

Chen, Y., Lu, L.-Q., Yu, D.-G., Zhu, C.-J., and Xiao, W.-J. (2018). Visible light-driven organic photochemical synthesis in China. Sci. China Chem. *62*, 24–57.

Cismesia, M.A., and Yoon, T.P. (2015). Characterizing chain processes in visible light photoredox catalysis. Chem. Sci. *6*, 5426–5434.

Courant, T., and Masson, G. (2016). Recent progress in visible-light photoredox-catalyzed intermolecular 1,2-difunctionalization of double bonds via an ATRA-type mechanism. J. Org. Chem. *81*, 6945–6952.

Crouch, R.D. (1994). The Ritter reaction: trapping a carbocation with a nitrile. J. Chem. Educ. *71*, A200–A202.

Dauncey, E.M., Morcillo, S.P., Douglas, J.J., Sheikh, N.S., and Leonori, D. (2018). Photoinduced remote functionalisations by iminyl radical promoted C-C and C-H bond cleavage cascades. Angew. Chem. Int. Ed. *57*, 744–748.

Eren, T., and Kusefoglu, S.H. (2005). Synthesis and polymerization of the acrylamide derivatives of fatty compounds. J. Appl. Polym. Sci. *97*, 2264–2272.

Feng, C., Li, Y., Sheng, X., Pan, L., and Liu, Q. (2018). A Ritter-type route to *N*-benzylamides by multicomponent reaction based on *p*-(trifluoromethyl)-*p*-quinols. Org. Lett. *20*, 6449–6452.

Fumagalli, G., Boyd, S., and Greaney, M.F. (2013). Oxyarylation and aminoarylation of styrenes using photoredox catalysis. Org. Lett. *15*, 4398–4401.

Giedyk, M., Goliszewska, K., ó Proinsias, K., and Gryko, D. (2016). Cobalt(I)-catalysed CH-alkylation of terminal olefins, and beyond. Chem. Commun. *52*, 1389–1392.

Guérinot, A., Reymond, S., and Cossy, J. (2012). Ritter reaction: Recent catalytic developments. Eur. J. Org. Chem. 19–28.

Gurjar, J., and Fokin, V.V. (2020). Sulfuryl fluoride mediated synthesis of amides and amidines from ketoximes via Beckmann rearrangement. Chem. Eur. J. *26*, 10402–10405.

Hatchard, C.G., and Parker, C.A. (1956). A new sensitive chemical actinometer. II. Potassium ferrioxalate as a standard chemical actinometer. Proc. R. Soc. Lond. Ser. A. *235*, 518–536.

Hopkinson, M.N., Tlahuext-Aca, A., and Glorius, F. (2016). Merging visible light photoredox and gold catalysis. Acc. Chem. Res. *49*, 2261–2272.

Huang, J.-M., Ye, Z.-J., Chen, D.-S., and Zhu, H. (2012). Iodine mediated/Brønsted acid-catalyzed dimerization of vinylarenes: a tandem reaction through Ritter trapping to produce *N*-(4-iodo-1,3-diarylbutyl) acetamides. Org. Biomol. Chem. *10*, 3610–3612.

Isse, A.A., and Gennaro, A. (2004). Homogeneous reduction of haloacetonitriles by electrogenerated aromatic radical anions: determination of the reduction potential of $\cdot CH_2CN$. J. Phys. Chem. A. *108*, 4180–4186.

Ji, D.-W., Hu, Y.-C., Zheng, H., Zhao, C.-Y., Chen, Q.-A., and Dong, V.-M. (2019). A regioselectivity switch in Pd-catalyzed hydroallylation of alkynes. Chem. Sci. *10*, 6311–6315.

Jiang, D., He, T., Ma, L., and Wang, Z. (2014). Recent developments in Ritter reaction. RSC Adv. *4*, 64936–64946.

Jiang, H., and Studer, A. (2020). Intermolecular radical carboamination of alkenes. Chem. Soc. Rev. *49*, 1790–1811.

Jiang, W.-S., Jiang, X.-L., Ji, D.-W., Zhang, W.-S., Zhang, G., Min, X.-T., Hu, Y.-C., and Chen, Q.-A. (2021). Orthogonal regulation of nucleophilic and electrophilic sites in Pd-catalyzed regiodivergent couplings between indazoles and isoprene. Angew. Chem. Int. Ed. *60*, 8321–8328.

Koike, T., and Akita, M. (2016). A versatile strategy for difunctionalization of carbon-carbon multiple bonds by photoredox catalysis. Org. Chem. Front. *3*, 1345–1349.

Kuai, C.S., Ji, D.-W., Zhao, C.-Y., Liu, H., Hu, Y.-C., and Chen, Q.-A. (2020). Ligand-regulated regiodivergent hydrosilylation of isoprene under iron catalysis. Angew. Chem. Int. Ed. *59*, 19115–19120.

Kuhn, H.J., Braslavsky, S.E., and Schmidt, R. (2004). Chemical actinometry (IUPAC technical report). Pure Appl. Chem. *76*, 2105–2146.

Kürti, L., and Czakó, B. (2005). Strategic Applications of Named Reactions in Organic Synthesis (Elsevier Inc).

Li-Zhulanov, N.S., Pavlova, A.V., Korchagina, D.V., Gatilov, Y.V., Volcho, K.P., Tolstikova, T.G., and Salakhutdinov, N.F. (2020). Synthesis of 1,3-oxazine derivatives based on (–)-isopulegol using the Ritter reaction and study of their analgesic activity. Chem. Heterocycl. Compd. *56*, 936–941.

Lipp, A., Badir, S.O., and Molander, G.A. (2021). Stereoinduction in metallaphotoredox catalysis. Angew. Chem. Int. Ed. *60*, 1714–1726.

Liu, S., and Klussmann, M. (2020). Acid promoted radical-chain difunctionalization of styrenes with stabilized radicals and (N,O)-nucleophiles. Chem. Commun. *56*, 1557–1560.

Ma, X., He, Y., Wang, P., and Lu, M. (2012). The hydration of nitriles catalyzed by simple transition metal salt of the fourth period with the aid of acetaldoxime. Appl. Organometal. Chem. *26*, 377–382.

Magagnano, G., Gualandi, A., Marchini, M., Mengozzi, L., Ceroni, P., and Cozzi, P.G. (2017). Photocatalytic ATRA reaction promoted by iodo-bodipy and sodium ascorbate. Chem. Commun. *53*, 1591–1594.

Mao, L.-L., and Cong, H. (2017). Atom-transfer radical addition to unactivated alkenes by using heterogeneous visible-light photocatalysis. ChemSusChem *10*, 4461–4464.

Marzo, L., Pagire, S.K., Reiser, O., and König, B. (2018). Visible-light photocatalysis: does it make a difference in organic synthesis? Angew. Chem. Int. Ed. *57*, 10034–10072.

Min, X.-T., Ji, D.-W., Guan, Y.-Q., Guo, S.-Y., Hu, Y.-C., Wan, B., and Chen, Q.-A. (2021). Visible light induced bifunctional rhodium catalysis for decarbonylative coupling of imides with alkynes. Angew. Chem. Int. Ed. *60*, 1583–1587.

Mohammadi Ziarani, G., Soltani Hasankiadeh, F., and Mohajer, F. (2020). Recent applications of Ritter reactions in organic syntheses. ChemistrySelect *5*, 14349–14379.

Nandy, S., Das, A.K., and Bhar, S. (2020). Chemoselective formation of C–N bond in wet acetonitrile using Amberlyst®-15(H) as a Recyclable catalyst. Synth. Commun. *50*, 3326–3336.

Narayanam, J.M.R., and Stephenson, C.R.J. (2011). Visible light photoredox catalysis: applications in organic synthesis. Chem. Soc. Rev. *40*, 102–113.

Norell, J.R. (1970). Organic reactions in liquid hydrogen fluoride. II. Synthesis of imidoyl fluorides and *N,N'*-dialkyl-2-alkylaminomalon-amides. J. Org. Chem. *35*, 1619–1925.

Ouyang, X.-H., Song, R.-J., and Li, J.-H. (2018). Developments in the chemistry of α-carbonyl alkyl bromides. Chem. -Asian J. *13*, 2316–2332.

Park, S.W., Kim, S.-H., Song, J., Park, G.Y., Kim, D., Nam, T.-G., and Hong, K.B. (2018). Hypervalent iodine-mediated Ritter-type amidation of terminal alkenes: the synthesis of isoxazoline and pyrazoline cores. Beilstein J. Org. Chem. *14*, 1028–1033.

Prasad Hari, D., Hering, T., and König, B. (2014). The photoredox-catalyzed Meerwein addition reaction: intermolecular amino-arylation of alkenes. Angew. Chem. Int. Ed. *53*, 725–728.

Prier, C.K., Rankic, D.A., and MacMillan, D.W.C. (2013). Visible light photoredox catalysis with transition metal complexes: applications in organic synthesis. Chem. Rev. *113*, 5322–5363.

Pronin, S.V., Reiher, C.A., and Shenvi, R.A. (2013). Stereoinversion of tertiary alcohols to tertiary-alkyl isonitriles and amines. Nature *501*, 195–199.

Protti, S., Garbarino, S., Ravelli, D., and Basso, A. (2016). Photoinduced multicomponent reactions. Angew. Chem. Int. Ed. *55*, 15476–15484.

Pu, W., Sun, D., Fan, W., Pan, W., Chai, Q., Wang, X., and Lv, Y. (2019). Cu-Catalyzed atom transfer radical addition reactions of alkenes with alpha-bromoacetonitrile. Chem. Commun. *55*, 4821–4824.

Qian, B., Chen, S., Wang, T., Zhang, X., and Bao, H. (2017). Iron-catalyzed carboamination of olefins: synthesis of amines and disubstituted beta-amino acids. J. Am. Chem. Soc. *139*, 13076–13082.

Qu, G.-R., Song, Y.-W., Niu, H.-Y., Guo, H.-M., and Fossey, J.S. (2012). $Cu(OTf)_2$-catalysed Ritter reaction: efficient synthesis of amides from nitriles and halohydrocarbons in water. RSC Adv. *2*, 6161–6163.

Rawner, T., Lutsker, E., Kaiser, C.A., and Reiser, O. (2018). The different faces of photoredox catalysts: visible-light-mediated atom transfer radical addition (ATRA) reactions of perfluoroalkyl iodides with styrenes and phenylacetylenes. ACS Catal. *8*, 3950–3956.

Ritter, J.J., and Kalish, J. (1948). New reaction of nitriles. II. Synthesis of t-Carbinamines. J. Am. Chem. Soc. *70*, 4048–4050.

Ritter, J.J., and Minieri, P.P. (1948). New reaction of nitriles. I. Amides from alkenes and mononitriles. J. Am. Chem. Soc. *70*, 4045–4048.

Romero, N.A., and Nicewicz, D.A. (2016). Organic photoredox catalysis. Chem. Rev. *116*, 10075–10166.

Rowe, J.E., Lee, K., Dolliver, D.D., and Johnson, J.E. (1999). Preparation of imidoyl fluorides. Aust. J. Chem. *52*, 807–811.

Shaw, M.H., Twilton, J., and MacMillan, D.W.C. (2016). Photoredox catalysis in organic chemistry. J. Org. Chem. *81*, 6898–6926.

Shi, R., Ai, W., He, T., Ma, X., Qian, S., and Wang, Z. (2015). An efficient way to synthesize *N*-(β-nitroalkyl) amides through Ritter reaction. Lett. Org. Chem. *12*, 720–726.

Shi, Y., Tan, X., Gao, S., Zhang, Y., Wang, J., Zhang, X., and Yin, Q. (2020). Direct synthesis of chiral NH lactams via Ru-catalyzed asymmetric reductive amination/cyclization cascade of keto acids/esters. Org. Lett. *22*, 2707–2713.

Shih, H.-W., Vander Wal, M.N., Grange, R.L., and MacMillan, D.W.C. (2010). Enantioselective α-benzylation of aldehydes via photoredox organocatalysis. J. Am. Chem. Soc. *132*, 13600–13603.

Skubi, K.L., Blum, T.R., and Yoon, T.P. (2016). Dual catalysis strategies in photochemical synthesis. Chem. Rev. *116*, 10035–10074.

Subba Reddy, B.V., Sivasankar Reddy, N., Madan, C., and Yadav, J.S. (2010). $HBF_4{\cdot}OEt_2$ as a mild and versatile reagent for the Ritter amidation of olefins: a facile synthesis of secondary amides. Tetrahedron Lett. *51*, 4827–4829.

Tellis, J.C., Kelly, C.B., Primer, D.N., Jouffroy, M., Patel, N.R., and Molander, G.A. (2016). Single-electron transmetalation via photoredox/nickel dual catalysis: unlocking a new paradigm for sp^3-sp^2 Cross-Coupling. Acc. Chem. Res. *49*, 1429–1439.

Twilton, J., Le, C., Zhang, P., Shaw, M.H., Evans, R.W., and MacMillan, D.W.C. (2017). The merger of transition metal and photocatalysis. Nat. Rev. Chem. *1*, 0052.

Welniak, M. (1996). The Ritter reaction of terpenes. Part 1. The isotricyclene system. Pol. J. Chem. *70*, 752–758.

Williams, S.G., Bhadbhade, M., Bishop, R., and Ung, A.T. (2017). An alkaloid-like 3-azabicyclo [3.3.1]non-3-ene library obtained from the bridged Ritter reaction. Tetrahedron *73*, 116–128.

Xu, S.-C., Zhu, S.-J., Chen, Y.-X., Wang, J., Bi, L.-W., Lu, Y.-J., Gu, Y., and Zhao, Z.-D. (2017). Skeletal rearrangement in the Ritter reaction of turpentine: a novel synthesis of *p*-menthane diamides. J. Chem. Res. *41*, 124–127.

Xuan, J., and Xiao, W.-J. (2012). Visible-light photoredox catalysis. Angew. Chem. Int. Ed. *51*, 6828–6838.

Yang, J., Ji, D.-W., Hu, Y.-C., Min, X.-T., Zhou, X., and Chen, Q.-A. (2019). Cobalt-catalyzed hydroxymethylarylation of terpenes with formaldehyde and arenes. Chem. Sci. *10*, 9560–9564.

Yang, L., Fan, W.X., Lin, E., Tan, D.H., Li, Q., and Wang, H. (2018). Synthesis of α-CF_3 and α-CF_2H amines via the aminofluorination of fluorinated alkenes. Chem. Commun. *54*, 5907–5910.

Yang, Z.F., Xu, C., Zheng, X., and Zhang, X. (2020). Nickel-catalyzed carbodifunctionalization of N-vinylamides enables access to gamma-amino acids. Chem. Commun. *56*, 2642–2645.

Yasu, Y., Koike, T., and Akita, M. (2013). Intermolecular aminotrifluoromethylation of alkenes by visible-light-driven photoredox catalysis. Org. Lett. *15*, 2136–2139.

Yasuda, K., and Obora, Y. (2015). $NbCl_5$-mediated amidation of olefins with nitriles to secondary amides. J. Organomet. Chem. *775*, 33–38.

Yi, H., Zhang, X., Qin, C., Liao, Z., Liu, J., and Lei, A. (2014). Visible light-induced γ-alkoxynitrile synthesis via three-component alkoxycyanomethylation of alkenes. Adv. Synth. Catal. *356*, 2873–2877.

Yin, Y., Zhao, X., and Jiang, Z. (2020). Advances in the synthesis of imine-containing azaarene derivatives via photoredox catalysis. ChemCatChem *12*, 4471–4489.

Yu, X.Y., Chen, J.R., and Xiao, W.J. (2021). Visible light-driven radical-mediated C-C bond cleavage/functionalization in organic synthesis. Chem. Rev. *121*, 506–561.

Yu, X.-Y., Zhao, Q.-Q., Chen, J., Xiao, W.-J., and Chen, J.-R. (2020). When light meets nitrogen-centered radicals: from reagents to catalysts. Acc. Chem. Res. *53*, 1066–1083.

Zhang, Y., Chen, S., Liu, Y., and Wang, Q. (2020). Route evaluation and Ritter reaction based synthesis of oxazoline acaricide candidates FET-II-L and NK-12. Org. Process. Res. Dev. *24*, 216–227.

Zheng, D., and Studer, A. (2019). Asymmetric synthesis of heterocyclic gamma-amino-acid and

diamine derivatives by three-component radical cascade reactions. Angew. Chem. Int. Ed. *58*, 15803–15807.

Zheng, Y., He, Y., Rong, G., Zhang, X., Weng, Y., Dong, K., Xu, X., and Mao, J. (2015). NaI-mediated acetamidosulphenylation of alkenes with nitriles as the nucleophiles: a direct access to acetamidosulfides. Org. Lett. *17*, 5444–5447.

Zhu, C., Yue, H., Chu, L., and Rueping, M. (2020). Recent advances in photoredox and nickel dual-catalyzed cascade reactions: pushing the boundaries of complexity. Chem. Sci. *11*, 4051–4064.

Zhu, N., Wang, T., Ge, L., Li, Y., Zhang, X., and Bao, H. (2017). γ-Amino butyric acid (GABA) synthesis enabled by copper-catalyzed carboamination of alkenes. Org. Lett. *19*, 4718–4721.

Zong, Y., Lang, Y., Yang, M., Li, X., Fan, X., and Wu, J. (2019). Synthesis of β-sulfonyl amides through a multicomponent reaction with the insertion of sulfur dioxide under visible light irradiation. Org. Lett. *21*, 1935–1938.

STAR★METHODS

KEY RESOURCES TABLE

REAGENT or RESOURCE	SOURCE	IDENTIFIER
Chemicals		
$Ir(ppy)_3$	Energy Chemical	Cat#94928-86-6
Eosin Y	TCI	Cat#17372-87-1
Styrene	Sinopharm Chemical Reagent Co. LTD	Cat#100-42-5
4-Bromostyrene	Accela ChemBio Co., Ltd.	Cat#2039-82-9
4-Chlorostyrene	Chembee	Cat#1073-67-2
3-Chlorostyrene	Alfa Aesar	Cat#2039-85-2
4-tert-Butylstyrene	Macklin	Cat#1746-23-2
4-Methylstyrene	TCI	Cat#622-97-9
4-Fluorostyrene	J&K Scientific	Cat#405-99-2
1-(Chloromethyl)-4-vinylbenzene	Energy Chemical	Cat#1592-20-7
4-Vinyl-1,1′-biphenyl	9Dingchem	Cat#2350-89-2
3-Methylstyrene	Energy Chemical	Cat#100-80-1
2-Bromostyrene	Innochem	Cat#2039-88-5
2-Chlorostyrene	Alfa Aesar	Cat#2039-87-4
Bromoacetonitrile	Accela ChemBio Co., Ltd.	Cat#590-17-0
Ethyl bromoacetate	Sinopharm Chemical Reagent Co. LTD	Cat#105-36-2
Ethyl 2-bromo-2-fluoro-acetate	Energy Chemical	Cat#401-55-8
Ethyl 2-bromo-2,2-difluoroacetate	Energy Chemical	Cat#667-27-6
Methyl 2-bromopropano-ate	Alfa Aesar	Cat#5445-17-0
Phenyl 2-bromoacetate	TCI	Cat#620-72-4
SuperDry acetonitrile	J&K Scientific	Cat#75-05-8
Benzonitrile	Sinopharm Chemical Reagent Co. LTD	Cat#100-47-0
o-Tolunitrile	Energy Chemical	Cat#529-19-1
m-Tolunitrile	Aladdin	Cat#620-22-4
3-Methylbutanenitrile	Acros	Cat#625-28-5
Valeronitrile	Sigma-Aldrich	Cat#110-59-8
Isobutyronitrile	TCI	Cat#78-82-0
Pivalonitrile	Energy Chemical	Cat#630-18-2
$NEt_3 \cdot 3HF$	Energy Chemical	Cat#73602-61-6
Potassium fluoride	Aladdin	Cat#7789-23-3
Cesium fluoride	Energy Chemical	Cat#13400-13-0
Deposited data		
CIF of 6b	CCDC 2039204	https://www.ccdc.cam.ac.uk/structures/
Other		
Blue LED lamps (40W, peak wavelength of 456 nm)	GeAo Chemical	http://www.geaochem.com/
Silica gel (200-300 mesh)	Xinchengsilicagel	http://www.ytsilica-gel.com
thin layer chromatography using TLC silica gel plates with phosphomolybdic acid chromogenic agent	Xinchengsilicagel	http://www.ytsilica-gel.com

(*Continued on next page*)

Continued

REAGENT or RESOURCE	SOURCE	IDENTIFIER
AVANCE III 400 MHz	Bruker	https://bruker.com
AVAVCE III HD 700 MHz	Bruker	https://bruker.com
X-ray diffraction	Agilent GeminiUltra	https://www.agilent.com.cn/
HRMS data of new compounds	Agilent Q-TOF 6540 & Agilent 8890-7250 GC/Q-TOF	https://www.agilent.com.cn/
UV/Vis absorption spectra	Lambda 950	https://www.perkinelmer.com.cn/

RESOURCE AVAILABILITY

Lead contact

Further information and requests for resources should be directed to and will be fulfilled by the lead contact, Qing-An Chen (qachen@dicp.ac.cn).

Materials availability

All other data supporting the findings of this study are available within the article and the supplemental information or from the lead contact upon reasonable request.

Data and code availability

Crystallographic data for the structures reported in this article have been deposited at the Cambridge Crystallographic Data Centre (CCDC) under accession numbers CCDC 2039204 (**6b**). Copies of the data can be obtained free of charge from https://www.ccdc.cam.ac.uk/structures/. All other data are available from the Lead Contact upon reasonable request.

METHOD DETAILS

Initial trials and reaction optimization (see Table S1)

In the glove box, styrene **1a** (0.21 mmol) and bromoacetonitrile **2a** (0.20 mmol) were added to a solution of additive (0.40 mmol) and $Ir(ppy)_3$ (0.002 mmol, 1.0 mol%) in acetonitrile (0.8 mL). Subsequently, the reaction mixture was stirred under the irradiation of 10-W blue light-emitting diodes (LEDs) at room temperature for 12 h. After the reaction completed and was quenched by H_2O, yield was determined by ^1H NMR analysis of crude mixture using 1,3,5-trimethoxybenzene (8.4 mg, 0.05 mmol) as an internal standard.

General procedure A

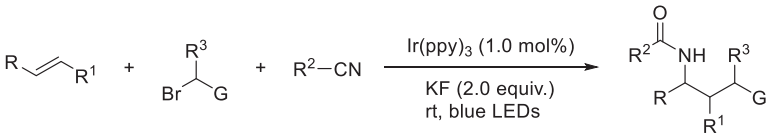

In the glove box, alkenes **1** (0.21 mmol) and radical precursors **2** (0.20 mmol) were added to a solution of KF (0.40 mmol) and $Ir(ppy)_3$ (0.002 mmol, 1.0 mol%) in nitriles (0.8 mL). Subsequently, the reaction mixture was stirred under the irradiation of 10-W blue LEDs at room temperature for 12 h. The reaction was quenched by exposure to air, with reaction mixture added into 0.5 mL water and extracted with EtOAc (3 x 5 mL). The combined organic layers were dried over Na_2SO_4, filtered, and concentrated in vacuo. The crude residue was purified by flash chromatography on silica gel (petroleum ether/ethyl acetate: 8/1-1/1 v/v) to afford products **3** (Zhu et al., 2017), **6**, **8**.

Light on/off experiments

According to the photo-induced condition (Table S1, entry 6), a reaction containing naphthalene as an internal standard was set up and placed in a blue LED reactor. The reaction was sequentially stirred under visible light irradiation and in the absence of light. Every 30 s, an aliquot of 10 μL was collected via syringe and analyzed by GC-FID. After 240 s, the determined yields were plotted against the reaction time (see Table S2, Figure S81).

Quantum yield measurements

$$\text{mol } Fe^{2+} = \frac{V \cdot \Delta A}{1 \cdot \varepsilon} = \frac{0.00235\text{L} \cdot 0.0361}{1.000 \text{ cm} \cdot 11\ 100 \text{ L mol}^{-1} \text{ cm}^{-1}} = 7.6428 \times 10^{-9}\text{mol} \quad \text{Equation 1}$$

$$f = 1 - 10^{-A} = 1 - 10^{-3.5968} = 0.9997 \quad \text{Equation 2}$$

$$\text{photo flux} = \frac{\text{mol } Fe^{2+}}{\Phi \cdot t \cdot f} = \frac{7.6428 \times 10^{-9} \text{ mol}}{1.01 \cdot 90.0 \text{ s} \cdot 0.9997} = 8.41 \times 10^{-11} \text{ einstein s}^{-1} \quad \text{Equation 3}$$

The photon flux of the spectrophotometer was determined by standard ferrioxalate actinometry (Cismesia and Yoon, 2015; Hatchard and Parker, 1956; Kuhn et al., 2004). A 0.15 M solution of ferrioxalate was prepared by dissolving 2.21 g of potassium ferrioxalate hydrate in 30 mL of 0.05 M H_2SO_4. A buffered solution of phenanthroline was prepared by dissolving 50 mg of phenanthroline and 11.25 g of sodium acetate in 50 mL of 0.5 M H_2SO_4. Both solutions were stored in dark. To determine the photon flux of the spectrophotometer, 2.0 mL of the ferrioxalate solution was placed in a cuvette and irradiated for 90.0 s at λ = 436 nm with an emission slit width at 2.0 nm. After irradiation, 0.35 mL of the phenanthroline solution was added to the cuvette. The solution was then allowed to rest for 1 h to allow the ferrous ions to completely coordinate to the phenanthroline. The absorbance of the solution was measured at 510 nm. A nonirradiated sample was also prepared, and the absorbance at 510 nm measured. Conversion was calculated using Equation 1, where V is the total volume (0.00235 L) of the solution after addition of phenanthroline, ΔA is the difference in absorbance at 510 nm between the irradiated and nonirradiated solutions, l is the path length (1.000 cm), and ε is the molar absorptivity at 510 nm (11,100 L mol^{-1} cm^{-1}) (Hatchard and Parker, 1956). The photon flux can be calculated using Equation 3, where Φ is the quantum yield for the ferrioxalate actinometer (1.01 for a 0.15 M solution at λ = 436 nm) (Hatchard and Parker, 1956), t is the time (90.0 s), and f is the fraction of light absorbed at λ = 436 nm (0.9997, Equation 2) (see Figure S82).

$$f = 1 - 10^{-A} = 1 - 10^{-1.4210} = 0.962$$

$$\Phi = \frac{\text{mol(TM)}}{\text{photo flux} \cdot t \cdot f} = \frac{1.56 \cdot (0.42/99.58) \cdot 9.4 \cdot 10^{-3}/202.1}{8.41 \times 10^{-11} \text{ einstein s}^{-1} \cdot 3 \cdot 3600 \text{ s} \cdot 0.962} = 0.35 \quad \text{Equation 4}$$

A cuvette was charged with styrene **1a** (0.21 mmol), and bromoacetonitrile **2a** (0.20 mmol) was added to a solution of KF (0.30 mmol) and $Ir(ppy)_3$ (0.001 mmol, 0.5 mol%) in acetonitrile (3.0 mL). The cuvette was then capped with a polytetrafluoroethylene stopper. The sample was stirred and irradiated (λ = 436 nm, slit width = 2.0 nm) for 10,800 s (3 h). After irradiation, internal standard (naphthalene, 9.4 mg) was added. The yield of product formed was determined by GC-FID. The quantum yield was determined using Equation 4 (see Figure S83).

Characterization of products 3a-3o

N-(3-cyano-1-phenylpropyl)acetamide (3a).

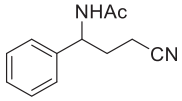

According to the general procedure A. Known compound, white solid, mp 95–96°C, 36.9 mg, 91% yield, R_f= 0.3 (petroleum ether/EtOAc 1/1). **^{1}H NMR** (400 MHz, $CDCl_3$) δ 7.37–7.26 (m, 5H), 6.53 (d, *J* = 8.0 Hz, 1H),

5.04–4.99 (m, 1H), 2.34–2.31 (m, 2H), 2.24–2.15 (m, 1H), 2.15–2.07 (m, 1H), 1.97 (s, 3H). **^{13}C NMR** (100 MHz, $CDCl_3$) δ 170.0, 140.1, 129.0, 128.1, 126.4, 119.3, 52.7, 31.6, 23.1, 14.4.

N-(3-cyano-1-(p-tolyl)propyl)acetamide (**3b**).

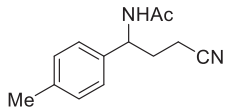

According to the general procedure A. Known compound, white solid, mp 103–104°C, 36.0 mg, 83% yield, R_f = 0.2 (petroleum ether/EtOAc 1/1). **^{1}H NMR** (400 MHz, $CDCl_3$) δ 7.19–7.15 (m, 4H), 6.11 (d, *J* = 7.8 Hz, 1H), 5.02–4.96 (m, 1H), 2.35–2.30 (m, 5H), 2.27–2.20 (m, 1H), 2.12–2.07 (m, 1H), 1.98 (s, 3H). **^{13}C NMR** (100 MHz, $CDCl_3$) δ 169.8, 138.0, 136.9, 129.7, 126.4, 119.3, 52.5, 31.6, 23.3, 21.0, 14.4.

N-(1-(4-(tert-butyl)phenyl)-3-cyanopropyl)acetamide (3c).

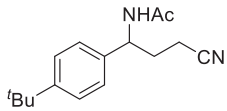

According to the general procedure A. Known compound, white solid, mp 125–126°C, 43.5 mg, 84% yield, R_f = 0.4 (petroleum ether/EtOAc 1/1). **^{1}H NMR** (400 MHz, $CDCl_3$) δ 7.39 (d, *J* = 8.3 Hz, 2H), 7.21 (d, *J* = 8.2 Hz, 2H), 5.89 (d, *J* = 7.2 Hz, 1H), 5.05–4.99 (m, 1H), 2.36–2.29 (m, 2H), 2.29–2.21 (m, 1H), 2.17–2.10 (m, 1H), 1.99 (s, 3H), 1.31 (s, 9H). **^{13}C NMR** (100 MHz, $CDCl_3$) δ 169.7, 151.3, 136.8, 126.2, 126.0, 119.3, 52.4, 34.5, 31.6, 31.2, 23.3, 14.5.

N-(1-([1,1′-biphenyl]-4-yl)-3-cyanopropyl)acetamide (**3d**).

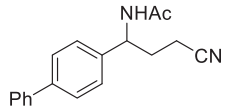

According to the general procedure A. Known compound, white solid, mp 197–198°C, 46.2 mg, 83% yield, R_f = 0.1 (petroleum ether/EtOAc 1/1). **^{1}H NMR** (400 MHz, DMSO-d_6) δ 8.40 (d, *J* = 8.4 Hz, 1H), 7.66–7.63 (m, 4H),7.46 (t, *J* = 7.6 Hz, 2H), 7.41–7.34 (m, 3H), 4.94–4.88 (m, 1H), 2.54–2.48 (m, 2H), 2.03–1.97 (m, 2H), 1.89 (s, 3H). **^{13}C NMR** (100 MHz, DMSO-d_6) δ 169.4, 142.1, 140.4, 139.5, 129.4, 127.8, 127.5, 127.2, 127.1, 120.7, 51.7, 31.9, 23.2, 14.5.

N-(3-cyano-1-(4-fluorophenyl)propyl)acetamide (**3e**).

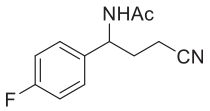

According to the general procedure A. Known compound, white solid, mp 122–123°C, 36.6 mg, 83% yield, R_f = 0.4 (petroleum ether/EtOAc 1/1). **^{1}H NMR** (400 MHz, $CDCl_3$) δ 7.28–7.25 (m, 2H), 7.08–7.03 (m, 2H), 6.11 (d, *J* = 8.0 Hz, 1H), 5.06–5.01 (m, 1H), 2.36 (t, *J* = 7.3 Hz, 2H), 2.27–2.17 (m, 1H), 2.15–2.06 (m, 1H), 2.00 (s, 3H). **^{13}C NMR** (100 MHz, $CDCl_3$) δ 169.8, 162.3 (d, *J* = 247.3 Hz), 135.9 (d, *J* = 3.3 Hz),128.2 (d, *J* = 8.1 Hz), 119.1, 116.0 (d, *J* = 21.5 Hz), 52.1, 31.6, 23.3, 14.5. **^{19}F NMR** (376 MHz, $CDCl_3$) δ −113.53.

N-(1-(4-chlorophenyl)-3-cyanopropyl)acetamide (**3f**).

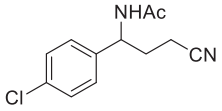

According to the general procedure A. Known compound, white solid, mp 148–149°C, 45.0 mg, 95% yield, R_f = 0.4 (petroleum ether/EtOAc 1/1). **^{1}H NMR** (400 MHz, $CDCl_3$) δ 7.35–7.33 (m, 2H), 7.24–7.21 (m, 2H), 6.23 (d, *J* = 7.6 Hz, 1H), 5.05–4.99 (m, 1H), 2.36 (t, *J* = 7.3 Hz, 2H), 2.24–2.16 (m, 1H), 2.14–2.07 (m, 1H), 2.00 (s, 3H). **^{13}C NMR** (100 MHz, $CDCl_3$) δ 169.9, 138.6, 134.0, 129.2, 127.9, 119.1, 52.1, 31.4, 23.2, 14.5.

N-(1-(4-bromophenyl)-3-cyanopropyl)acetamide (**3g**).

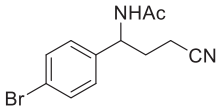

According to the general procedure A. Known compound, off-white solid, mp 144–145°C, 55.3 mg, 98% yield, R_f = 0.3 (petroleum ether/EtOAc 1/1). **^{1}H NMR** (400 MHz, $CDCl_3$) δ 7.49 (d, *J* = 8.4 Hz, 2H), 7.16 (d, *J* = 8.3 Hz, 2H), 6.30 (d, *J* = 8.2 Hz, 1H), 5.03–4.98 (m, 1H), 2.36 (t, *J* = 7.4 Hz, 2H), 2.22–2.04 (m, 2H), 1.99 (s, 3H). **^{13}C NMR** (100 MHz, $CDCl_3$) δ 170.0, 139.3, 132.2, 128.3, 122.1, 119.2, 52.2, 31.4, 23.3, 14.5.

N-(1-(4-(chloromethyl)phenyl)-3-cyanopropyl)acetamide (**3h**).

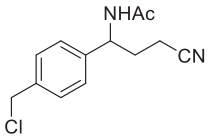

According to the general procedure A. Known compound, white solid, mp 131–132°C, 41.9 mg, 84% yield, R_f = 0.2 (petroleum ether/EtOAc 1/1). **^{1}H NMR** (400 MHz, $CDCl_3$) δ 7.39 (d, *J* = 8.2 Hz, 2H), 7.28 (d, *J* = 6.2 Hz, 2H), 6.33 (d, *J* = 7.1 Hz, 1H), 5.07–5.01 (m, 1H), 4.57 (s, 2H), 2.34 (t, *J* = 7.4 Hz, 2H), 2.22–2.08 (m, 2H), 1.98 (s, 3H). **^{13}C NMR** (100 MHz, $CDCl_3$) δ 169.9, 140.4, 137.4, 129.3, 126.9, 119.2, 52.4, 45.6, 31.5, 23.2, 14.5.

N-(3-cyano-1-(m-tolyl)propyl)acetamide (**3i**).

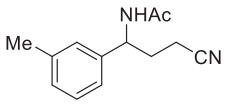

According to the general procedure A. Known compound, white solid, mp 96–98°C, 36.6 mg, 85% yield, R_f = 0.2 (petroleum ether/EtOAc 1/1). **^{1}H NMR** (400 MHz, $CDCl_3$) δ 7.27–7.22 (m, 1H), 7.12–7.06 (m, 3H), 6.38 (d, *J* = 8.1 Hz, 1H), 5.00–4.95 (m, 1H), 2.34 (s, 3H), 2.33–2.30 (m, 2H), 2.23–2.18 (m, 1H), 2.13–2.06 (m, 1H), 1.98 (s, 3H). **^{13}C NMR** (100 MHz, $CDCl_3$) δ 169.8, 139.9, 138.8, 128.9, 128.8, 127.3, 123.3, 119.3, 52.7, 31.6, 23.2, 21.3, 14.4.

N-(1-(3-chlorophenyl)-3-cyanopropyl)acetamide (**3j**).

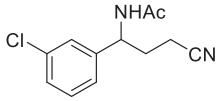

According to the general procedure A. Known compound, white solid, mp 117–118°C, 46.8 mg, 99% yield, R_f = 0.3 (petroleum ether/EtOAc 1/1). **^{1}H NMR** (400 MHz, $CDCl_3$) δ 7.31–7.26 (m, 3H), 7.18–7.16 (m, 1H), 6.74 (d, *J* = 8.2 Hz, 1H), 5.04–4.98 (m, 1H), 2.36 (t, *J* = 7.2 Hz, 2H), 2.20–2.05 (m, 2H), 1.99 (s, 3H). **^{13}C NMR** (100 MHz, $CDCl_3$) δ 170.1, 142.4, 134.8, 130.3, 128.2, 126.5, 124.8, 119.1, 52.2, 31.5, 23.1, 14.5.

N-(1-(2-chlorophenyl)-3-cyanopropyl)acetamide (**3k**).

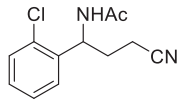

According to the general procedure A. Known compound, white solid, mp 128–129°C, 42.4 mg, 90% yield, R_f= 0.3 (petroleum ether/EtOAc1/1). **^{1}H NMR** (400 MHz, $CDCl_3$) δ 7.38–7.36 (m, 1H), 7.33–7.31 (m, 1H), 7.28–7.21 (m, 2H), 6.85 (d, *J* = 8.3 Hz, 1H), 5.42–5.36 (m, 1H), 2.45–2.36 (m, 2H), 2.20–2.10 (m, 2H), 2.00 (s, 3H). **^{13}C NMR** (100 MHz, $CDCl_3$) δ 170.0, 137.8, 132.7, 130.2, 129.1, 127.8, 127.4, 119.2, 50.6, 30.6, 23.1, 14.5.

N-(1-(2-bromophenyl)-3-cyanopropyl)acetamide (**3l**).

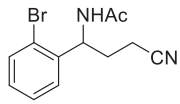

According to the general procedure A. Unknown compound, white solid, mp 134–135°C, 52.9 mg, 94% yield, R_f = 0.2 (petroleum ether/EtOAc 1/1). **^{1}H NMR** (400 MHz, DMSO-d_6) δ 8.50 (d, *J* = 8.1 Hz, 1H), 7.59 (d, *J* = 8.0 Hz, 1H), 7.44–7.37 (m, 2H), 7.23–7.19 (m, 1H), 5.20–5.15 (m, 1H), 2.59 (t, *J* = 7.0 Hz, 2H), 1.98–1.92 (m, 1H), 1.90 (s, 3H), 1.85–1.76 (m, 1H). **^{13}C NMR** (100 MHz, DMSO-d_6) δ 169.6, 142.2, 133.1, 129.6, 128.6, 127.8, 122.6, 120.3, 51.6, 31.0, 23.1, 14.5. **HRMS** calculated for $C_{12}H_{14}BrN_2O^+$ $[M + H]^+$ 281.0284, found: 281.0281.

N-(3-cyano-1-(naphthalen-2-yl)propyl)acetamide (**3m**).

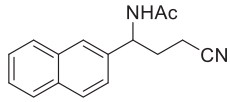

According to the general procedure A. Known compound, white solid, mp 137–139°C, 23.8 mg, 47% yield, R_f = 0.1 (petroleum ether/EtOAc 1/1). **^{1}H NMR** (400 MHz, $CDCl_3$) δ 7.84–7.78 (m, 3H), 7.72 (s, 1H), 7.50–7.48 (m, 2H), 7.36 (dd, *J* = 8.5, 1.6 Hz, 1H), 6.31 (d, *J* = 8.1 Hz, 1H), 5.21–5.16 (m, 1H), 2.35–2.30 (m, 2H), 2.28–2.16 (m, 2H), 1.99 (s, 3H). **^{13}C NMR (100 MHz, $CDCl_3$)** δ 169.9, 137.2, 133.2, 132.9, 129.1, 127.8, 127.6, 126.6, 126.4, 125.5, 124.1, 119.3, 52.8, 31.4, 23.3, 14.5.

N-(2-(cyanomethyl)-2,3-dihydro-1*H*-inden-1-yl)acetamide (**3n**).

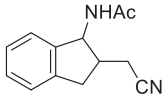

8:1 dr

According to the general procedure A. Known compound, white solid, mp 107–109°C, 35.6 mg, 83% yield, 8:1 dr, R_f = 0.3 (petroleum ether/EtOAc 1/1). **^{1}H NMR** (400 MHz, $CDCl_3$) δ 7.31–7.21 (m, 4.5H), 6.15 (d, *J* = 8.5 Hz, 0.13H), 6.01 (d, *J* = 8.0 Hz, 1H), 5.47–5.44 (m, 1H), 5.20–5.16 (m, 0.13H), 3.27–3.21 (m, 0.13H), 3.19–3.12 (m, 1H), 2.98–2.89 (m, 2H), 2.82–2.73 (m, 0.26H), 2.61–2.53 (m, 1.13H), 2.51–2.46 (m, 0.13H), 2.44–2.38 (m, 1H), 2.04 (s, 0.38H), 2.02 (s, 3H). **^{13}C NMR** (100 MHz, $CDCl_3$) δ 170.61, 170.55, 141.4, 141.2, 140.7, 140.6, 128.9, 128.5, 127.4, 127.3, 125.1, 124.8, 124.5, 123.5, 119.0, 118.5, 59.0, 56.2, 45.5, 39.3, 35.9, 35.7, 23.1, 22.9, 20.8, 17.9. **HRMS** calculated for $C_{13}H_{15}N_2O^+$ [M + H]$^+$ 215.1179, found 215.1184.

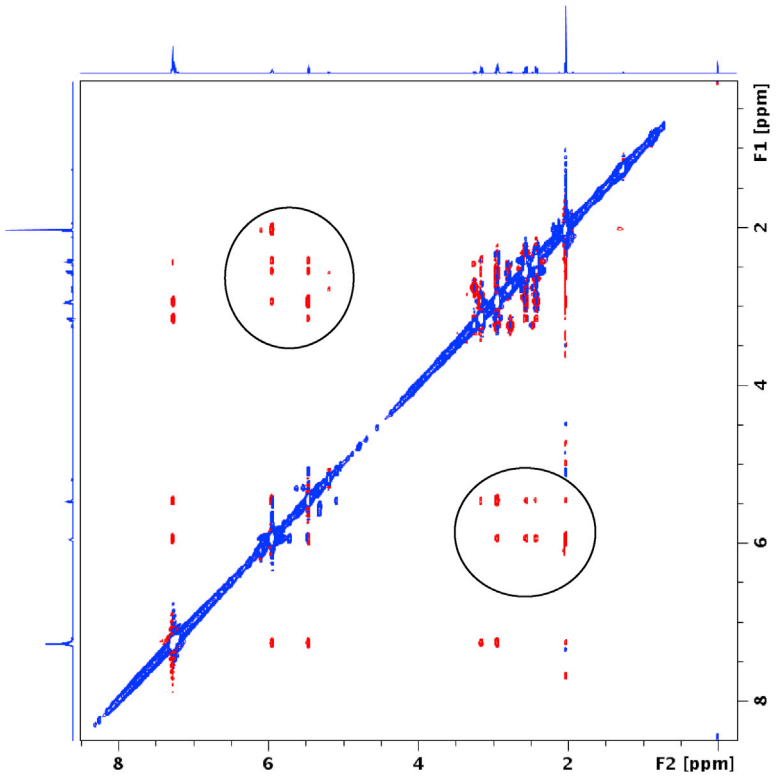

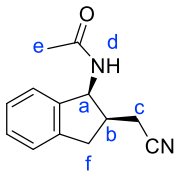

rac-**3n**, 8:1 dr

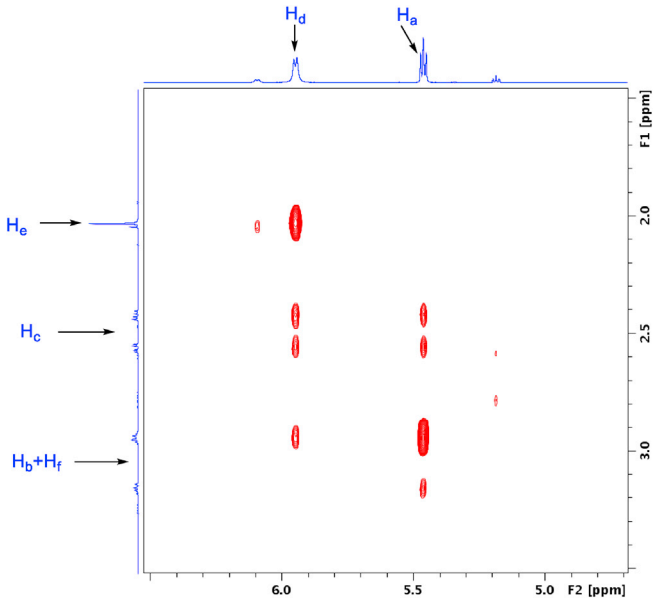

N-(3-cyano-2-methyl-1-phenylpropyl)acetamide (3o).

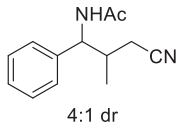

Prepared according to the general procedure A, KF (1.5 equiv., 17.4 mg); known compound, white solid, mp 95–97°C, 38.6 mg, 89% yield, 4:1 dr, R_f = 0.2 (petroleum ether/EtOAc 1/1.5). **^{1}H NMR** (400 MHz, $CDCl_3$) δ 7.36–7.23 (m, 6.15H), 6.72 (d, *J* = 9.0 Hz, 1.22H), 4.99–4.95 (m, 0.23H), 4.84–4.79 (m, 1H), 2.60–2.53 (m, 1H), 2.34–2.26 (m, 2.23H), 2.13–2.06 (m, 0.46H), 2.00 (s, 0.69H), 1.97 (s, 3H), 1.15 (d, *J* = 6.7 Hz, 0.69H), 0.96 (d, *J* = 6.4 Hz, 3H). **^{13}C NMR** (100 MHz, $CDCl_3$) δ 170.02, 169.97, 139.7, 139.5, 128.9, 128.9, 127.9, 126.9, 126.7, 119.2, 118.5, 57.8, 56.9, 36.1, 35.8, 23.2, 22.1, 21.7, 17.1, 15.6. **HRMS** calculated for $C_{13}H_{17}N_2O^+$ $[M + H]^+$ 217.1335, found 217.1337.

Characterization of products 6a–6k

Ethyl 4-acetamido-4-phenylbutanoate (6a).

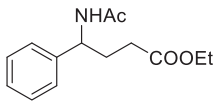

Prepared according to the general procedure A, KF (1.5 equiv., 17.4 mg); known compound (Giedyk et al., 2016), off-white solid, mp 116–117°C, 35.5 mg, 71% yield, R_f = 0.3 (petroleum ether/EtOAc 1/1). **^{1}H NMR** (400 MHz, $CDCl_3$) δ 7.35–7.23 (m, 5H), 6.31 (d, *J* = 8.0 Hz, 1H), 5.00–4.95 (m, 1H), 4.11 (q, *J* = 7.1 Hz, 2H), 2.40–2.26 (m, 2H), 2.19–2.05 (m, 2H), 1.95 (s, 3H), 1.24 (t, *J* = 7.1 Hz, 3H). **^{13}C NMR** (100 MHz, $CDCl_3$) δ 173.5, 169.4, 141.5, 128.7, 127.5, 126.4, 60.6, 53.1, 31.2, 30.8, 23.2, 14.1. **HRMS** calculated for $C_{14}H_{20}NO_3^+$ $[M + H]^+$ 250.1438, found 250.1445.

*Ethyl 4-acetamido-4-(4-bromophenyl)butanoate (**6b**).*

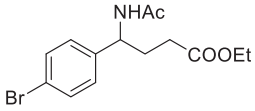

Prepared according to the general procedure A, KF (1.5 equiv., 17.4 mg); unknown compound, light yellow solid, mp 131–133°C, 37.2 mg, 57% yield, R_f = 0.3 (petroleum ether/EtOAc 1/1). **^{1}H NMR** (400 MHz, $CDCl_3$) δ 7.44 (d, *J* = 8.4 Hz, 2H), 7.15 (d, *J* = 8.4 Hz, 2H), 6.40 (d, *J* = 7.8 Hz, 1H), 4.95–4.89 (m, 1H), 4.12 (q, *J* = 7.1 Hz, 2H), 2.38–2.29 (m, 2H), 2.13–2.01 (m, 2H), 1.96 (s, 3H), 1.25 (t, *J* = 7.1 Hz, 3H). **^{13}C NMR** (100 MHz, $CDCl_3$) δ 173.5, 169.5, 140.8, 131.7, 128.2, 121.2, 60.7, 52.7, 31.1, 30.6, 23.2, 14.1. **HRMS** calculated for $C_{14}H_{19}BrNO_3^+$ $[M + H]^+$ 328.0543, found 328.0553.

*Ethyl 4-acetamido-4-(4-chlorophenyl)butanoate (**6c**).*

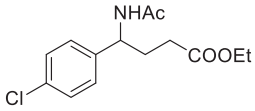

Prepared according to the general procedure A, KF (1.5 equiv., 17.4 mg); known compound, white solid, mp 112–113°C, 28.8 mg, 51% yield, Rf = 0.3 (petroleum ether/EtOAc 1/1). **^{1}H NMR** (400 MHz, $CDCl_3$) δ 7.31–7.27 (m, 2H), 7.22–7.20 (m, 2H), 6.37 (d, *J* = 7.8 Hz, 1H), 4.96–4.91 (m, 1H), 4.12 (q, *J* = 7.1 Hz, 2H), 2.38–2.29 (m, 2H), 2.15–2.01 (m, 2H), 1.96 (s, 3H), 1.25 (t, *J* = 7.1 Hz, 3H). **^{13}C NMR** (100 MHz, $CDCl_3$) δ 173.5, 169.5, 140.2, 133.2, 128.8, 127.8, 60.7, 52.6, 31.1, 30.6, 23.2, 14.1. **HRMS** calculated for $C_{14}H_{19}ClNO_3^+$ $[M + H]^+$ 284.1048, found 284.1055.

*Ethyl 4-acetamido-4-(3-chlorophenyl)butanoate (**6d**).*

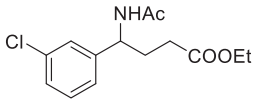

Prepared according to the general procedure A, KF (1.5 equiv., 17.4 mg); unknown compound, white solid, mp 77–79°C, 41.8 mg, 74% yield, R_f = 0.3 (petroleum ether/EtOAc 1/1). **^{1}H NMR** (400 MHz, $CDCl_3$) δ 7.27–7.21 (m, 3H), 7.17–7.15 (m, 1H), 6.46 (d, *J* = 7.9 Hz, 1H), 4.97–4.91 (m, 1H), 4.12 (q, *J* = 7.1 Hz, 2H), 2.39–2.30 (m, 2H), 2.13–2.02 (m, 2H), 1.97 (s, 3H), 1.25 (t, *J* = 7.1 Hz, 3H). **^{13}C NMR** (100 MHz, $CDCl_3$) δ 173.5, 169.6, 143.9, 134.5, 129.9, 127.6, 126.5, 124.8, 60.7, 52.8, 31.1, 30.7, 23.2, 14.1. **HRMS** calculated for $C_{14}H_{19}ClNO_3^+$ $[M + H]^+$ 284.1048, found 284.1055.

*Ethyl 4-acetamido-4-(2-bromophenyl)butanoate (**6e**).*

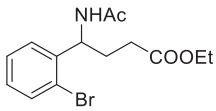

Prepared according to the general procedure A, KF (1.5 equiv., 17.4 mg); unknown compound, off-white solid, mp 75–77°C, 47.7 mg, 73% yield, R_f = 0.2 (petroleum ether/EtOAc 1/1). **^{1}H NMR** (400 MHz, $CDCl_3$) δ 7.53 (d, *J* = 8.0 Hz, 1H), 7.28–7.27 (m, 2H), 7.13–7.09 (m, 1H), 6.72 (d, *J* = 7.5 Hz, 1H), 5.29–5.24 (m, 1H), 4.13 (q, *J* = 7.1 Hz, 2H), 2.47–2.32 (m, 2H), 2.13–2.08 (m, 2H), 1.97 (s, 3H), 1.25 (t, *J* = 7.1 Hz, 3H). **^{13}C NMR** (100 MHz, $CDCl_3$) δ 173.8, 169.5, 140.7, 133.3, 128.8, 127.7, 127.6, 122.9, 60.7, 53.3, 31.2, 29.6, 23.1, 14.1. **HRMS** calculated for $C_{14}H_{19}BrNO_3^+$ $[M + H]^+$ 328.0543, found 328.0535.

*Ethyl 4-acetamido-2-fluoro-4-phenylbutanoate (**6f**).*

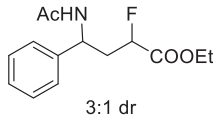

Prepared according to the general procedure A, KF (1.5 equiv., 17.4 mg); unknown compound, off-white solid, mp 82–83°C, 36.5 mg, 68% yield, 3:1 dr, R_f = 0.2 (petroleum ether/EtOAc 1/1). **^{1}H NMR** (400 MHz, $CDCl_3$) δ 7.37–7.25 (m, 5H), 6.49 (d, *J* = 8.3 Hz, 0.72H), 6.37 (d, *J* = 7.9 Hz, 0.24H), 5.35–5.30 (m, 0.73H), 5.27–5.21 (m, 0.25H), 4.92 (ddd, *J* = 49.0, 8.7, 4.1 Hz, 0.74H), 4.76 (ddd, *J* = 48.8, 8.8, 3.6 Hz, 0.25H), 4.23–4.17 (m, 2H), 2.42–2.30 (m, 2H), 1.99 (s, 2.20H), 1.94 (s, 0.74H), 1.30–1.26 (m, 3H). **^{13}C NMR** (100 MHz, $CDCl_3$) δ 169.6, 169.5, 169.4, 169.3, 140.6, 140.3, 128.9, 128.7, 127.9, 127.6, 126.6, 126.3, 86.9 (d, *J* = 184.0 Hz), 86.6 (d, *J* = 184.0 Hz), 61.75, 61.70, 50.5 (d, *J* = 2.5 Hz), 49.6 (d, *J* = 1.7 Hz), 38.5 (d, *J* = 20.4 Hz), 38.3 (d, *J* = 20.4 Hz), 23.22, 23.18, 14.0. **^{19}F NMR** (376 MHz, $CDCl_3$) δ −190.65, −191.54. **HRMS** calculated for $C_{14}H_{19}FNO_3^+$ $[M + H]^+$ 268.1343, found 268.1328.

*Ethyl 4-acetamido-2,2-difluoro-4-phenylbutanoate (**6g**).*

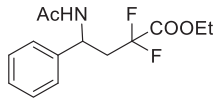

Prepared according to the general procedure A, KF (1.1 equiv., 12.8 mg); known compound (Yang et al., 2020), white solid, mp 59–61°C, 30.1 mg, 53% yield, R_f = 0.2 (petroleum ether/EtOAc 1/1). **^{1}H NMR** (400 MHz, $CDCl_3$) δ 7.36–7.27 (m, 5H), 6.00 (d, *J* = 7.7 Hz, 1H), 5.34–5.28 (m, 1H), 4.18 (q, *J* = 7.1 Hz, 2H), 2.78–2.53 (m, 2H), 1.96 (s, 3H), 1.31 (t, *J* = 7.2 Hz, 3H). **^{13}C NMR** (100 MHz, $CDCl_3$) δ 169.1, 163.7 (t, *J* = 32.3 Hz), 140.4, 128.8, 128.0, 126.4, 114.9 (t, *J* = 251.8 Hz), 63.1, 48.2 (t, *J* = 4.8 Hz), 40.2 (t, *J* = 22.8 Hz), 23.2, 13.8. **^{19}F NMR** (376 MHz, $CDCl_3$) δ −102.97, −103.05. **HRMS** calculated for $C_{14}H_{18}F_2NO_3^+$ $[M + H]^+$ 286.1249, found 286.1255.

*Ethyl 4-acetamido-4-(4-bromophenyl)-2,2-difluorobutanoate (**6h**).*

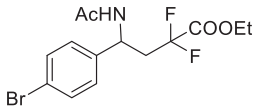

Prepared according to the general procedure A, KF (1.1 equiv., 12.8 mg); unknown compound, off-white solid, mp 97–98°C, 26.6 mg, 37% yield, R_f = 0.2 (petroleum ether/EtOAc 1/1). **^{1}H NMR** (400 MHz, $CDCl_3$) δ 7.46 (d, *J* = 8.4 Hz, 2H), 7.17 (d, *J* = 8.4 Hz, 2H), 6.20 (d, *J* = 7.8 Hz, 1H), 5.28–5.23 (m, 1H), 4.22 (q, *J* = 7.1 Hz, 2H), 2.73–2.48 (m, 2H), 1.96 (s, 3H), 1.32 (t, *J* = 7.2 Hz, 3H). **^{13}C NMR** (100 MHz, $CDCl_3$) δ 169.3, 163.6 (t, *J* = 32.0 Hz), 139.6, 131.9, 128.2, 121.8, 114.8 (t, *J* = 252.2 Hz), 63.3, 47.7 (t, *J* = 4.7 Hz), 39.9 (t, *J* = 22.8 Hz), 23.1, 13.8. **^{19}F NMR** (376 MHz, $CDCl_3$) δ −103.14. **HRMS** calculated for $C_{14}H_{17}BrF_2NO_3^+$ $[M + H]^+$ 364.0354, found 364.0352.

*Ethyl 4-acetamido-4-(2-bromophenyl)-2,2-difluorobutanoate (**6i**).*

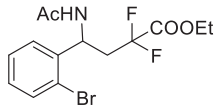

Prepared according to the general procedure A, KF (1.1 equiv., 12.8 mg); unknown compound, light yellow solid, mp 116–117°C, 42.1 mg, 58% yield, R_f = 0.2 (petroleum ether/EtOAc 1/1). **^{1}H NMR** (400 MHz, $CDCl_3$) δ 7.54 (dd, *J* = 8.0, 0.9 Hz, 1H), 7.35–7.28 (m, 2H), 7.15–7.11 (m, 1H), 6.53 (d, *J* = 7.7 Hz, 1H), 5.61–5.55 (m, 1H),

4.23 (q, *J* = 7.1 Hz, 2H), 2.72–2.61 (m, 2H), 1.98 (s, 3H), 1.33 (t, *J* = 7.1 Hz, 3H). **^{13}C NMR** (100 MHz, $CDCl_3$) δ 169.2, 163.5 (t, *J* = 32.3 Hz), 139.3, 133.5, 129.3, 128.4, 127.8, 122.4, 114.9 (t, *J* = 252.0 Hz), 63.2, 48.5 (t, *J* = 4.7 Hz), 38.6 (t, *J* = 22.9 Hz), 23.1, 13.8. **^{19}F NMR** (376 MHz, $CDCl_3$) δ −102.99, −103.04. **HRMS** calculated for $C_{18}H_{19}ClNO_3^+$ $[M + H]^+$ 364.0354, found 364.0354.

Methyl 4-acetamido-2-methyl-4-phenylbutanoate (6j).

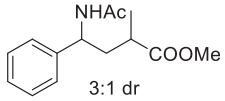

Prepared according to the general procedure A, KF (1.1 equiv., 12.8 mg); unknown compound, sticky oil, 22.2 mg, 45% yield, 3:1 dr, R_f = 0.2 (petroleum ether/EtOAc 1/1). **^{1}H NMR** (400 MHz, $CDCl_3$) δ 7.34–7.23 (m, 5H), 6.09 (d, *J* = 7.7 Hz, 0.27H), 5.98 (d, *J* = 8.4 Hz, 0.75H), 5.09–5.02 (m, 1H), 3.68 (s, 2.24H), 3.60 (s, 0.79H), 2.57–2.42 (m, 1H), 2.29–2.17 (m, 1H), 1.95–1.88 (m, 3.55H), 1.82–1.75 (m, 0.86H), 1.23–1.19 (m, 3H). **^{13}C NMR** (100 MHz, $CDCl_3$) δ 177.2, 176.7, 169.3, 169.1, 142.2, 141.3, 128.7, 128.7, 127.5, 127.4, 126.6, 126.3, 51.8, 39.8, 39.2, 37.2, 36.4, 23.31, 23.26, 17.7, 17.2. **HRMS** calculated for $C_{18}H_{19}ClNO_3^+$ $[M + H]^+$ 250.1438, found 250.1441.

Phenyl 4-acetamido-4-(3-chlorophenyl)butanoate (6k).

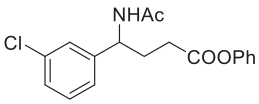

Prepared according to the general procedure A, KF (1.1 equiv., 12.8 mg); unknown compound, sticky oil, 41.5 mg, 63% yield, R_f = 0.2 (petroleum ether/EtOAc 1/1). **^{1}H NMR** (400 MHz, $CDCl_3$) δ 7.39–7.35 (m, 2H), 7.29–7.17 (m, 5H), 7.07–7.04 (m, 2H), 6.38 (d, *J* = 8.1 Hz, 1H), 5.07–5.01 (m, 1H), 2.63–2.56 (m, 2H), 2.21–2.14 (m, 2H), 1.96 (s, 3H). **^{13}C NMR** (100 MHz, $CDCl_3$) δ 172.0, 169.7, 150.5, 143.6, 134.6, 130.1, 129.4, 127.8, 126.5, 125.9, 124.8, 121.4, 52.6, 31.2, 30.6, 23.2. **HRMS** calculated for $C_{18}H_{19}ClNO_3^+$ $[M + H]^+$ 332.1048, found 332.1041.

Characterization of products 8a–8g

N-(3-cyano-1-phenylpropyl)benzamide (8a).

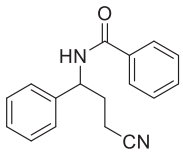

Prepared according to the general procedure A, 24 hr; unknown compound, white solid, mp 136–137°C, 24.3 mg, 46% yield, R_f = 0.5 (petroleum ether/EtOAc 2/1). **^{1}H NMR** (400 MHz, DMSO-d_6) δ 8.87 (d, *J* = 8.3 Hz, 1H), 7.90 (d, *J* = 7.6 Hz, 2H), 7.55 (t, *J* = 7.1 Hz, 1H), 7.48 (t, *J* = 7.5 Hz, 2H), 7.42–7.40 (m, 2H), 7.35 (t, *J* = 7.5 Hz, 2H), 7.26 (t, *J* = 7.0 Hz, 1H), 5.14–5.08 (m, 1H), 2.65–2.54 (m, 2H), 2.25–2.15 (m, 1H), 2.12–2.04 (m, 1H). **^{13}C NMR** (100 MHz, DMSO-d_6) δ 166.6, 143.3, 134.8, 131.8, 128.9, 128.7, 127.9, 127.6, 126.9, 120.7, 52.8, 31.7, 14.7. **HRMS** calculated for $C_{17}H_{17}N_2O^+$ $[M + H]^+$ 265.1335, found 265.1335.

N-(3-cyano-1-phenylpropyl)-2-methylbenzamide (8b).

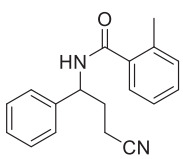

Prepared according to the general procedure A, CsF (2.0 equiv., 60.8 mg), 27 h; unknown compound, white solid, mp 117–118°C, 26.1 mg, 47% yield, R_f = 0.5 (petroleum ether/EtOAc 2/1). **^{1}H NMR** (400 MHz, $CDCl_3$) δ 7.42–7.29 (m, 7H), 7.21–7.16 (m, 2H), 6.16 (d, *J* = 7.6 Hz, 1H), 5.24–5.18 (m, 1H), 2.44–2.32 (m, 6H), 2.27–2.18 (m, 1H). **^{13}C NMR** (100 MHz, $CDCl_3$) δ 169.6, 139.7, 136.2, 135.7, 131.1, 130.2, 129.3, 128.4, 126.6, 126.5, 125.8, 119.1, 53.1, 31.7, 19.8, 14.5. **HRMS** calculated for $C_{18}H_{19}N_2O^+$ $[M + H]^+$ 279.1492, found 279.1489.

N-(3-cyano-1-phenylpropyl)-3-methylbenzamide (**8c**).

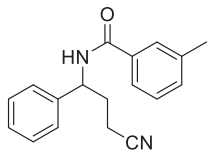

Prepared according to the general procedure A, CsF (2.0 equiv., 60.8 mg), 27 h; unknown compound, white solid, mp 97–99°C, 24.0 mg, 43% yield, R_f = 0.7 (petroleum ether/EtOAc 1/1). **^{1}H NMR** (400 MHz, $CDCl_3$) δ 7.58 (s, 1H), 7.55–7.53 (m, 1H), 7.41–7.29 (m, 7H), 6.59 (d, *J* = 7.9 Hz, 1H), 5.27–5.21 (m, 1H), 2.40–2.33 (m, 6H), 2.29–2.20 (m, 1H). **^{13}C NMR** (100 MHz, $CDCl_3$) δ 167.3, 139.9, 138.5, 133.9, 132.5, 129.2, 128.5, 128.3, 127.7, 126.5, 123.9, 119.3, 53.1, 31.7, 21.3, 14.5. **HRMS** calculated for $C_{18}H_{19}N_2O^+$ $[M + H]^+$ 279.1492, found 279.1501.

N-(3-cyano-1-phenylpropyl)isobutyramide (**8d**).

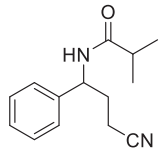

Prepared according to the general procedure A, CsF (2.0 equiv., 60.8 mg), 27 h; unknown compound, white solid, mp 113–115°C, 22.6 mg, 49% yield, R_f = 0.4 (petroleum ether/EtOAc 1/1). **^{1}H NMR** (400 MHz, $CDCl_3$) δ 7.39–7.27 (m, 5H), 5.99 (d, *J* = 7.8 Hz, 1H), 5.07–5.01 (m, 1H), 2.41–2.31 (m, 3H), 2.28–2.21 (m, 1H), 2.19–2.11 (m, 1H), 1.17 (d, *J* = 6.9 Hz, 3H), 1.12 (d, *J* = 6.9 Hz, 3H). **^{13}C NMR** (100 MHz, $CDCl_3$) δ 176.7, 140.1, 129.1, 128.1, 126.4, 119.3, 52.4, 35.6, 31.7, 19.5, 19.4, 14.4. **HRMS** calculated for $C_{14}H_{19}N_2O^+$ $[M + H]^+$231.1492, found 231.1486.

N-(3-cyano-1-phenylpropyl)pentanamide (**8e**).

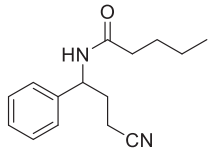

Prepared according to the general procedure A, CsF (2.0 equiv., 60.8 mg); unknown compound, white solid, mp 59–60°C, 22.4 mg, 46% yield, R_f = 0.6 (petroleum ether/EtOAc 1/1). **^{1}H NMR** (400 MHz, $CDCl_3$) δ 7.40–7.27 (m, 5H), 5.83 (d, *J* = 7.6 Hz, 1H), 5.08–5.03 (m, 1H), 2.36–2.10 (m, 6H), 1.65–1.57 (m, 2H), 1.37–1.28 (m, 2H), 0.90 (t, *J* = 7.3 Hz, 3H). **^{13}C NMR** (100 MHz, $CDCl_3$) δ 172.8, 140.0, 129.2, 128.2, 126.5, 119.3, 52.6, 36.4, 31.7, 27.6, 22.3, 14.5, 13.7. **HRMS** calculated for $C_{15}H_{21}N_2O^+$ $[M + H]^+$ 245.1648, found 245.1647.

N-(3-cyano-1-phenylpropyl)-3-methylbutanamide (**8f**).

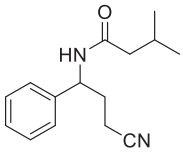

Prepared according to the general procedure A, 27 h; unknown compound, white solid, mp 80–81°C, 22.3 mg, 46% yield, R_f = 0.6 (petroleum ether/EtOAc 1/1). **^{1}H NMR** (400 MHz, $CDCl_3$) δ 7.39–7.37 (m, 5H), 5.99 (d, *J* = 7.8 Hz, 1H), 5.08–5.02 (m, 1H), 2.35–2.28 (m, 2H), 2.28–2.03 (m, 5H), 0.94 (d, *J* = 6.2 Hz, 3H), 0.91 (d, *J* = 6.2 Hz, 3H). **^{13}C NMR** (100 MHz, $CDCl_3$) δ 172.2, 140.0, 129.1, 128.2, 126.5, 119.2, 52.6, 45.9, 31.6, 26.1, 22.40, 22.36, 14.5. **HRMS** calculated for $C_{15}H_{21}N_2O^+$ $[M + H]^+$ 245.1648, found 245.1654.

N-(3-cyano-1-phenylpropyl)pivalamide (**8g**).

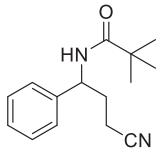

Prepared according to the general procedure A, CsF (2.0 equiv., 60.8 mg), 27 h; unknown compound, white solid, 15.4 mg, 32% yield, R_f = 0.3 (petroleum ether/EtOAc 2/1). **^{1}H NMR** (400 MHz, $CDCl_3$) δ 7.40–7.37 (m, 2H), 7.34–7.32 (m, 1H), 7.30–7.26 (m, 2H), 5.94 (d, *J* = 7.4 Hz, 1H), 5.07–5.02 (m, 1H), 2.35–2.29 (m, 2H), 2.27–2.13 (m, 2H), 1.21 (s, 9H). **^{13}C NMR** (100 MHz, $CDCl_3$) δ 178.1, 140.1, 129.2, 128.1, 126.3, 119.4, 52.6, 38.8, 31.7, 27.4, 14.4. **HRMS** calculated for $C_{15}H_{21}N_2O^+$ $[M + H]^+$ 245.1648, found 245.1649.

Gram-scale reaction

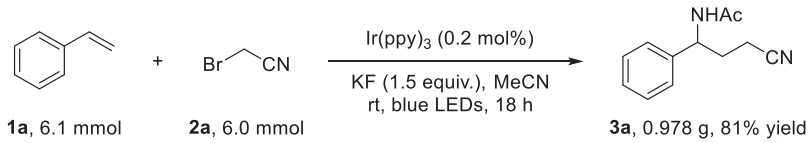

1a, 6.1 mmol **2a**, 6.0 mmol **3a**, 0.978 g, 81% yield

In the glove-box, styrene **1a** (6.1 mmol) and bromoacetonitrile **2a** (6.0 mmol) was added to a solution of KF (9.0 mmol) and $Ir(ppy)_3$ (0.012 mmol, 0.2 mol%) in acetonitrile (8.0 mL). Subsequently, the reaction mixture was stirred under the irradiation of 10 W blue LEDs at room temperature for 18 h. After the reaction completed, the crude product was purified by flash chromatography on silica gel (petroleum ether/ethyl acetate: 8/1-1/1 v/v) to afford the corresponding product **3a** (0.978 g, 81% yield).

Synthetic transformations

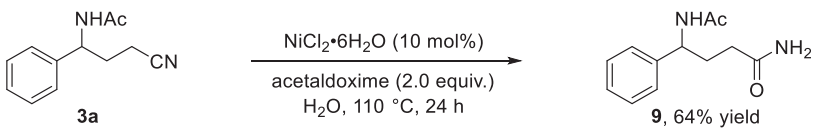

3a **9**, 64% yield

To a 25 mL round-bottom flask equipped with magnetic stirrer were added **3a** (0.5 mmol, 1 equiv.), acetaldoxime (1 mmol, 2 equiv.), nickel(II) chloride hexahydrate (0.05 mmol) and H_2O (5 mL). The mixture was

heated to reflux for 24 h. After cooling to room temperature, the solution was directly evaporated to dryness and the residue was purified by column chromatography on silica gel (ethyl acetate/*n*-hexane = 1:1) to give 4-acetamido-4-phenylbutanamide **9** (66.2 mg, 64%) as white solid (Ma et al., 2012). Unknown compound, **^{1}H NMR** (400 MHz, CD_3OD) δ 7.36–7.32 (m, 4H), 7.29–7.23 (m, 1H), 4.91–4.88 (m, 1H), 2.31–2.18 (m, 2H), 2.09–2.03 (m, 2H), 1.99 (s, 3H); **^{13}C NMR** (100 MHz, CD_3OD) δ 176.7, 171.3, 142.3, 128.2, 126.9, 126.2, 53.1, 32.0, 31.8, 21.3. **HRMS** calculated for $C_{12}H_{17}N_2O_2^+$ $[M + H]^+$ 221.1285, found 221.1296.

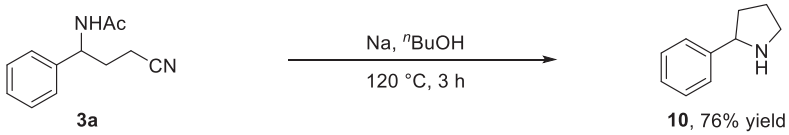

Na (8.0 mmol, 40 equiv.), ^{n}BuOH (1.0 mL) and 3a (0.20 mmol, 1 equiv.) were added into a flame-dried Schlenk tube with a stirring bar under nitrogen. The reaction mixture was heated to 120°C for 1 h. Then, ^{n}BuOH (1 mL) and Na (4.0 mmol, 20 equiv.) were added into the reaction and continued the reaction at 120°C for another 2 h. Then, the reaction mixture was cooled to ambient temperature. The reaction solution was washed by water and extraction with (30 mL × 3) CH_2Cl_2. The organic layer was dried over magnesium sulfate, filtered and concentrated by rotary evaporator under reduced pressure and the residue was purified by column chromatography on silica gel (PE/EA = 50/50-0/100) to yield 2-phenylpyrrolidine 10 (22.4 mg, 76%) as colorless oil. Known compound (Zhu et al., 2017), ^{1}H NMR (400 MHz, $CDCl_3$) δ 7.37–7.29 (m, 4H), 7.25–7.21 (m, 1H), 4.11 (t, *J* = 7.7 Hz, 1H), 3.24–3.18 (m, 1H), 3.04–2.98 (m, 1H), 2.23–2.15 (m, 1H), 2.05–2.02 (m, 1H), 1.97–1.80 (m, 2H), 1.72–1.63 (m, 1H); ^{13}C NMR (100 MHz, $CDCl_3$) δ 144.8, 128.3, 126.7, 126.5, 62.6, 47.0, 34.3, 25.6.

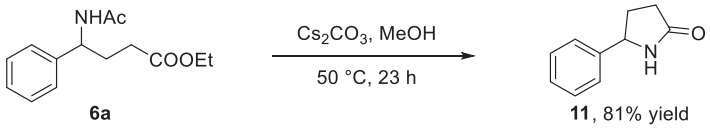

To a stirred solution of **6a** (0.1 mmol) in CH_3OH (1.0 mL) was added Cs_2CO_3 (0.15 mmol, 1.5 equiv) at room temperature and the mixture was stirred at 50°C for 23 hours. After completion of reaction as checked by TLC, the solvent was evaporated and the residue was purified directly by flash column chromatograph (petroleum ether/ethyl acetate, 1:1 v/v) to give 5-phenylpyrrolidin-2-one **11** (13.1 mg, 81%) as white solid (Zheng and Studer, 2019). Known compound (Shi et al., 2020), **^{1}H NMR** (400 MHz, $CDCl_3$) δ 7.39–7.35 (m, 2H), 7.31–7.29 (m, 3H), 6.37 (s, 1H), 4.75 (t, *J* = 7.1 Hz, 1H), 2.62–2.53 (m, 1H), 2.51–2.36 (m, 2H), 2.02–1.95 (m, 1H); **^{13}C NMR** (100 MHz, $CDCl_3$) δ 178.5, 142.5, 128.9, 127.9, 125.6, 58.0, 31.3, 30.3.

Mechanistic study

Radical trapping experiment.

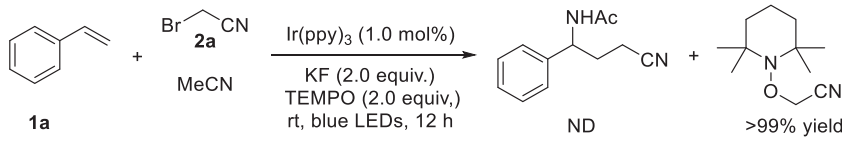

In the glove box, styrene 1a (0.21 mmol) and bromoacetonitrile **2a** (0.20 mmol) were added to a solution of KF (0.40 mmol), $Ir(ppy)_3$ (0.002 mmol, 1.0 mol%), and TEMPO (0.40 mmol, 2.0 equiv.) in acetonitrile (0.8 mL). Subsequently, the reaction mixture was stirred under the irradiation of 10-W blue LEDs at room temperature for 12 h. After the reaction completed, yield was determined by ^{1}H NMR analysis of crude mixture using 1,3,5-trimethoxybenzene (8.4 mg, 0.05 mmol) as an internal standard (see Figures S86 and S87).

Deuterium labeling experiment.

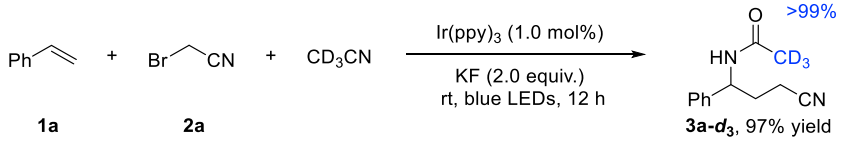

1a **2a** **3a-d_3**, 97% yield

In the glove box, styrene **1a** (0.21 mmol) and bromoacetonitrile **2a** (0.20 mmol) were added to a solution of KF (0.40 mmol) and $Ir(ppy)_3$ (0.002 mmol, 1.0 mol%) in CD_3CN (0.8 mL). Subsequently, the reaction mixture was stirred under the irradiation of 10-W blue LEDs at room temperature for 12 h. After the reaction completed, the crude product was purified by flash chromatography on silica gel (petroleum ether/ethyl acetate, 8/1-1/1 v/v) to afford the corresponding product **3a-d_3** (39.9 mg, 97% yield). **^{1}H NMR** (400 MHz, $CDCl_3$) δ 7.38–7.26 (m, 5H), 6.49 (d, *J* = 8.0 Hz, 1H), 5.05–4.99 (m, 1H), 2.34–2.30 (m, 2H), 2.25–2.15 (m, 1H), 2.15–2.07 (m, 1H). **^{2}D NMR** (700 MHz, $CDCl_3$) δ 1.97. **^{13}C NMR** (100 MHz, $CDCl_3$) δ 170.0, 140.1, 129.0, 128.1, 126.4, 119.3, 52.6, 31.6, 22.8–22.0 (m), 14.4. **HRMS** calculated for $C_{12}H_{12}D_3N_2O^+$ $[M + H]^+$ 206.1367, found 206.1367 (see Figure S88).

Heteroatom nucleophiles.

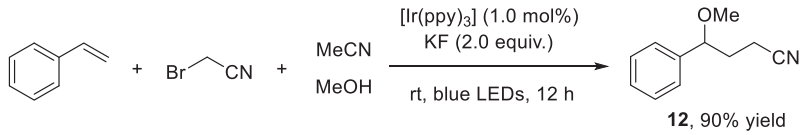

12, 90% yield

In the glove box, styrene **1a** (0.21 mmol) and bromoacetonitrile **2a** (0.20 mmol) were added to a solution of KF (0.40 mmol) and $Ir(ppy)_3$ (0.002 mmol, 1.0 mol%) in CH_3CN/MeOH (0.4 mL/0.4 mL). Subsequently, the reaction mixture was stirred under the irradiation of 10-W blue LEDs at room temperature for 12 h. After the reaction completed, yield was determined by ^{1}H NMR analysis of crude mixture using 1,3,5-trimethoxybenzene (8.4 mg, 0.05 mmol) as an internal standard. Compared with reported literature (Yi et al., 2014), 4-methoxy-4-phenylbutanenitrile was obtained with 90% yield (see Figure S89).

Control experiments

General procedure B.

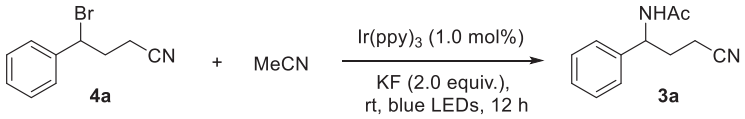

4a **3a**

In the glove box, 4-bromo-4-phenylbutanenitrile **4a** (0.20 mmol) was added to a solution of KF (0.40 mmol) and $Ir(ppy)_3$ (0.002 mmol, 1.0 mol%) in CH_3CN (0.8 mL). Subsequently, the reaction mixture was stirred under the irradiation of 10-W blue LEDs at room temperature for 12 h. After the reaction completed, the crude product was purified by flash chromatography on silica gel (petroleum ether/ethyl acetate, 8/1-1/1 v/v) to afford the corresponding product (see Table S4).

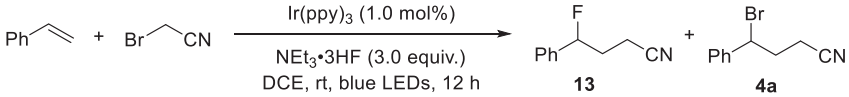

13 **4a**

75%, **13**:**4a** 2.5:1

In the glove box, styrene **1a** (0.21 mmol) and bromoacetonitrile **2a** (0.20 mmol) were added to a solution of $NEt_3 \cdot 3HF$ (0.60 mmol) and $Ir(ppy)_3$ (0.002 mmol, 1.0 mol%) in DCE (0.8 mL). Subsequently, the reaction

mixture was stirred under the irradiation of 10-W blue LEDs at room temperature for 12 h. After the reaction completed, the crude product was purified by flash chromatography on silica gel (petroleum ether/ethyl acetate, 12/1-10/1 v/v) to afford the corresponding product (75% yield, **13**:**4a** 2.5:1) (Dauncey et al., 2018) (see Figures S90 and S91).

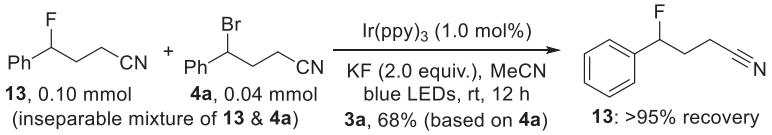

In the glove box, 4-fluoro-4-phenylbutanenitrile **13** (0.10 mmol) and **4a** (0.04 mmol) were added to a solution of KF (0.40 mmol) and $Ir(ppy)_3$ (0.0014 mmol, 1.0 mol%) in CH_3CN (0.6 mL). Subsequently, the reaction mixture was stirred under the irradiation of 10-W blue LEDs at room temperature for 12 h. After the reaction completed, yield was determined by ^1H NMR analysis of crude mixture using 1,3,5-trimethoxybenzene (8.4 mg, 0.05 mmol) as an internal standard (see Figure S92).

^{19}F NMR of reaction profiles. In the glove box, styrene **1a** (0.21 mmol) and bromoacetonitrile **2a** (0.20 mmol) were added to a solution of KF (0.40 mmol) and $Ir(ppy)_3$ (0.002 mmol, 1.0 mol%) in CH_3CN (0.8 mL). Subsequently, the reaction mixture was stirred under the irradiation of 10-W blue LEDs at room temperature. After the reaction completed, ^{19}F NMR was tested after quenching by H_2O (see Figure S93).

In the glove box, styrene **1a** (0.21 mmol) and bromoacetonitrile **2a** (0.20 mmol) were added to a solution of KF (0.40 mmol) and $Ir(ppy)_3$ (0.002 mmol, 1.0 mol%) in CH_3CN (0.8 mL). Subsequently, the reaction mixture was stirred under the irradiation of 10-W blue LEDs at room temperature for 10 min. Then, with additional D_2O, ^1H NMR, ^{13}C NMR, ^{19}F NMR, HMQC and HMBC was tested (see Figures S94–S98). **HRMS** calculated for $C_{12}H_{13}FN_2^+$ $[M]^+$ 204.1057, found 204.1060. In addition, using CD_3CN instead of CH_3CN, the same procedure was conducted to further confirm the structure of the intermediate (see Figures S99–S103). Furthermore, spectra of 10 min reaction time with the standard condition quenched by H_2O (20 μL) were also tested (see Figures S104–S106).

Further transformation of imidoyl fluoride. In the glove box, styrene **1a** (0.21 mmol) and bromoacetonitrile **2a** (0.20 mmol) were added to a solution of KF (0.40 mmol) and $Ir(ppy)_3$ (0.002 mmol, 1.0 mol%) in CH_3CN (0.8 mL). Subsequently, the reaction mixture was stirred under the irradiation of 10-W blue LEDs at room temperature for 12 h. Then, *N*-methylbenzylamine (0.22 mmol) was added to the mixture in the glove box, stirring at rt for 26 h. Next, yield of *N*-benzyl-*N*′-(3-cyano-1-phenylpropyl)-*N*- methylacetimidamide **14** (see Figures S107 and S108) was determined by ^1H NMR spectroscopy using 1,3,5-trimethoxy-benzene (8.4 mg, 0.05 mmol) as the internal standard. **HRMS** calculated for $C_{20}H_{24}N_3^+$ $[M + H]^+$ 306.1965, found 306.1960.